

Distributed Integrated Sensing and Communications: Foundations, Opportunities, and Challenges

George C. Alexandropoulos, Ph.D.

Associate Professor, *IEEE Senior Member*

IEEE ICC, Montreal, Canada

June 8, 2025



**National
and Kapodistrian
University of Athens**

Established in 1827

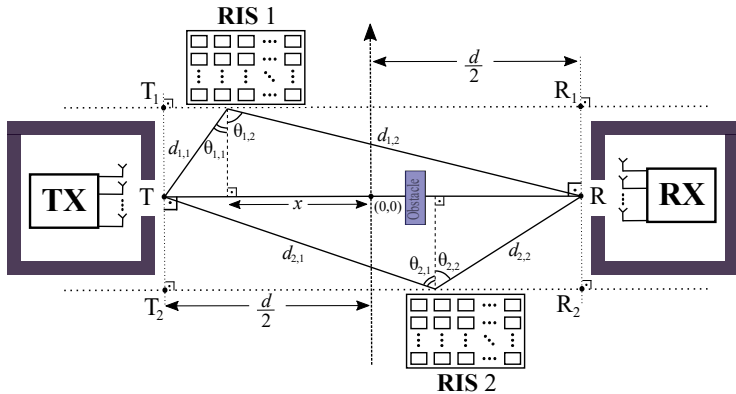


**Department of
Informatics and Telecommunications**

1 Part III: Distributed Sensing-Aided Communications

- Optimization of Multi-RIS-Aided Communications
- Distributed Learning for Multi-RIS-Aided Communications
- Position-Aided Near-Field Beam Tracking
- Sensing-Aided Communications via Hydrid RISs
- Over-the-Air Learning: The XL MIMO Potential

Multi-RIS-Empowered P2P Communications



A. L. Moustakas, G. C. Alexandropoulos, and M. Debbah, "Capacity optimization using reconfigurable intelligent surfaces: A large system approach," *IEEE GLOBECOM*, 2021.

A. L. Moustakas, G. C. Alexandropoulos, and M. Debbah, "Reconfigurable intelligent surfaces and capacity optimization: A large system analysis," *IEEE TWC*, 2023.

The MIMO-RIS Channel

- The received signal vector at RX: $\mathbf{y} \triangleq \sqrt{\rho} \mathbf{G}_{\text{tot}} (\{\Phi_k\}_{k=1}^K) \mathbf{x} + \mathbf{z}$.
- The e2e channel gain matrix: $\mathbf{G}_{\text{tot}} (\{\Phi_k\}_{k=1}^K) \triangleq \mathbf{G}_d + \sum_{k=1}^K \sqrt{\gamma_k} \mathbf{G}_{r,k} \Phi_k \mathbf{G}_{t,k}$ with γ_k modeling the relative additional SNR from each k -th RIS and $[\Phi_k]_{n,n} \triangleq e^{i\phi_{k,n}}$.
- Complex Gaussian channel matrices having the following Kronecker-product-form covariances $\forall i, j = 1, 2, \dots, N_r$, $\forall m, n = 1, 2, \dots, N_t$, and $\forall a, b = 1, 2, \dots, N_s$:

$$\mathbb{E} [[\mathbf{G}_d]_{i,m} [\mathbf{G}_d]_{j,n}^*] = \frac{1}{N_t} [\mathbf{R}_d]_{i,j} [\mathbf{T}_d]_{m,n},$$

$$\mathbb{E} [[\mathbf{G}_{r,k}]_{i,a} [\mathbf{G}_{r,k}]_{j,b}^*] = \frac{\delta_{k,k'}}{N_t} [\mathbf{R}_k]_{i,j} [\mathbf{S}_{r,k}]_{a,b},$$

$$\mathbb{E} [[\mathbf{G}_{t,k}]_{a,m} [\mathbf{G}_{t,k}]_{b,n}^*] = \frac{\delta_{k,k'}}{N_t} [\mathbf{S}_{t,k}]_{a,b} [\mathbf{T}_k]_{m,n}.$$

A. L. Moustakas, G. C. Alexandropoulos, and M. Debbah, "Reconfigurable intelligent surfaces and capacity optimization: A large system analysis," *IEEE TWC*, 2023.

Modeling of the Correlation Matrices

- The correlated electric fields at any location \mathbf{x}_a of an element a , $\forall a = 1, 2, \dots, N_s$, on each RIS are represented as an integral over random incoming or outgoing waves, each denoted by the 3-dimensional wave vector \mathbf{k} with magnitude $|\mathbf{k}| = k_0 \triangleq \frac{2\pi}{\lambda}$.
- The amplitude of the electric field in the integrand is weighted by the relative amplitude of radiation, $\sqrt{w_{r,k}(\mathbf{k})}$, in each wave direction and a corresponding phase factor $e^{i\mathbf{k}^T \mathbf{x}_a}$ referring to the a -th RIS element.
Averaging over randomness, each (a, b) -element of the matrix $\mathbf{S}_{r,k} \forall k$:

$$[\mathbf{S}_{r,k}]_{ab} = \int w_{r,k}(\mathbf{k}) e^{i\mathbf{k}^T (\mathbf{x}_a - \mathbf{x}_b)} d\Omega_{\mathbf{k}}.$$

- The integral is taken over all directions of \mathbf{k}/k_0 on the unit sphere with differential solid angle $d\Omega_{\mathbf{k}}$, and $w_{r,k}(\mathbf{k})$ is normalized so that, when $\mathbf{x}_a = \mathbf{x}_b$, the integral gives unity.

A. L. Moustakas, G. C. Alexandropoulos, and M. Debbah, "Reconfigurable intelligent surfaces and capacity optimization: A large system analysis," *IEEE TWC*, 2023.

The Generic Weight Function $w(\mathbf{k})$

- It represents the relative power arriving (or departing) from direction \mathbf{k} .
- In general, it depends on the distribution of the significant spatially resolved paths as well as the reflectance and polarization properties of the corresponding scatterers.
- For a given mean direction of arrival (or departure) \mathbf{s}_0 (with $|\mathbf{s}_0| = k_0$) and a standard deviation of the incoming (or outgoing) power characterized by the AS σ (in radians), $w(\mathbf{k})$ can be expressed as:

$$w(\mathbf{k}) \propto e^{-\frac{|\mathbf{k}-\mathbf{s}_0|^2}{2\sigma^2 k_0^2}}.$$

- $w(\mathbf{k})$ can be also expressed in terms of $\mathbf{k}_{||}$, the component of \mathbf{k} parallel to the RIS, and k_z , the component of \mathbf{k} perpendicular to the RIS: $w(\mathbf{k}_{||}, k_z)$.

A. L. Moustakas, G. C. Alexandropoulos, and M. Debbah, "Reconfigurable intelligent surfaces and capacity optimization: A large system analysis," *IEEE TWC*, 2023.

Closed-Form Ergodic MI Formula

- In the limit $N_t, N_r, N_s \rightarrow \infty$ with fixed ratios $\beta_r \triangleq N_r/N_t$ and $\beta_s \triangleq N_s/N_t$, the ergodic MI per TX antenna element takes the closed form:

$$\begin{aligned} C = & \frac{1}{N_t} \sum_{k=1}^K \log \det (\mathbf{I}_{N_s} + t_{1k} r_{2k} \gamma_k \boldsymbol{\Sigma}_k) + \frac{1}{N_t} \log \det (\mathbf{I}_{N_r} + \tilde{\mathbf{R}}) \\ & + \frac{1}{N_t} \log \det (\mathbf{I}_{N_t} + \rho \mathbf{Q} \tilde{\mathbf{T}}) - r_d t_d - \sum_{k=1}^K (r_{1k} t_{1k} + r_{2k} t_{2k}), \end{aligned}$$

where the parameters $r_{1k}, t_{1k}, r_{2k}, t_{2k}, r_d, t_d$ are the unique solutions of some fixed point equations and:

$$\begin{aligned} \tilde{\mathbf{R}} &\triangleq r_d \mathbf{R}_d + \sum_{k=1}^K r_{1k} \mathbf{R}_k, \quad \tilde{\mathbf{T}} \triangleq t_d \mathbf{T}_d + \sum_{k=1}^K t_{2k} \mathbf{T}_k, \\ \boldsymbol{\Sigma}_k &\triangleq \mathbf{S}_{t,k}^{1/2} \boldsymbol{\Phi}_k^\dagger \mathbf{S}_{r,k} \boldsymbol{\Phi}_k \mathbf{S}_{t,k}^{1/2}. \end{aligned}$$

A. L. Moustakas, G. C. Alexandropoulos, and M. Debbah, "Reconfigurable intelligent surfaces and capacity optimization: A large system analysis," *IEEE TWC*, 2023.

Inspection of the Ergodic MI Formula

- A key simplification in the asymptotic limit is the decoupling of the phase configuration matrices Φ_k 's of the different RISs; these matrices appear in separate $\log \det(\cdot)$ terms.

- MI's distribution converges weakly to a Gaussian:

$$\lim_{N_t \rightarrow \infty} \frac{I - N_t C}{\sqrt{\log \det(\Lambda^{-1})}} \sim \mathcal{N}(0, 1)$$

(recall that $I \triangleq \log \det (\mathbf{I}_{N_r} + \rho \mathbf{G}_{\text{tot}} (\{\Phi_k\}_{k=1}^K) \mathbf{Q} \mathbf{G}_{\text{tot}}^H (\{\Phi_k\}_{k=1}^K))$ and $C = \mathbb{E}[I]/N_t$).

- Maximizing C over the input covariance matrix \mathbf{Q} with the constraint of a fixed trace, i.e., $\text{Tr}\{\mathbf{Q}\} = N_t$, will give the ergodic capacity per antenna of the system for fixed Φ_k 's.

A. L. Moustakas, G. C. Alexandropoulos, and M. Debbah, "Reconfigurable intelligent surfaces and capacity optimization: A large system analysis," *IEEE TWC*, 2023.

Asymptotic Properties of the Correlation Matrices

- In the limit of the RISs' sizes increasing without bound, the eigenvectors of $\mathbf{S}_{t,k}$'s and $\mathbf{S}_{r,k}$'s essentially become Fourier modes, and their eigenvalues converge to the Fourier transforms of any line of the matrix.
- This observation showcases the relationship of this result with the so-called ***holographic concept***, according to which the EM modes of a 2D surface are related with the incoming (or outgoing) plane waves onto the surface:

Each incoming wavevector \mathbf{k} , with $|\mathbf{k}| = k_0$, corresponds to the eigenvector which has the same projection $\mathbf{q} = \mathbf{k}_{\parallel}$ on the plane of the RIS and a vertical component given by $\pm k_z(\mathbf{q})$.

A. L. Moustakas, G. C. Alexandropoulos, and M. Debbah, "Reconfigurable intelligent surfaces and capacity optimization: A large system analysis," *IEEE TWC*, 2023.

A. L. Moustakas, "Communication through a diffusive medium: Coherence and capacity," *Science*, 2000.

A. Pizzo, L. Sanguinetti, and T. L. Marzetta, "Fourier plane-wave series expansion for holographic MIMO communications," *IEEE TWC*, 2022.

L. Wei, C. Huang, G. C. Alexandropoulos, W. E. I. Sha, C. Yuen, Z. Zhang, and M. Debbah, "Holographic MIMO surfaces for multi-user communications: Channel modeling and spectral efficiency analysis," *IEEE JSTSP*, 2022.

Capacity Optimization Formulation

- We consider the optimization problem:

$$\begin{aligned}\mathcal{OP}_1 : \max_{\substack{\{\Phi_k\}_{k=1}^K, \\ \{d_{k,1}, d_{k,2}\}_{k=1}^K}} \quad & C \left(\{\Phi_k\}_{k=1}^K, \{d_{k,1}, d_{k,2}\}_{k=1}^K \right) \\ \text{s.t.} \quad & |[\Phi_k]_{n,n}| = 1 \quad \forall k, n.\end{aligned}$$

- Alternating optimization: keep $d_{k,1}$'s and $d_{k,2}$'s fixed to first find the Φ_k 's that maximize the ergodic MI; then, solve \mathcal{OP}_1 with respect to $d_{k,1}$'s and $d_{k,2}$'s using the previously optimized RIS phase configurations.
- In the large system limit, \mathcal{OP}_1 can be applied to both the ergodic and the outage capacity optimizations; MI's variance per TX antenna is $\text{Var}(I)/N_t^2$, and therefore, it vanishes.

A. L. Moustakas, G. C. Alexandropoulos, and M. Debbah, "Reconfigurable intelligent surfaces and capacity optimization: A large system analysis," *IEEE TWC*, 2023.

Closed-Form Solution for Φ_k 's (1/3)

- The multi-RIS phase configuration design problem can be simplified:

$$\begin{aligned}\mathcal{OP}_2 : \quad & \sum_{k=1}^K \max_{\{\Phi_k\}_{k=1}^K} \log \det \left(\mathbf{I}_{N_s} + t_{1k} r_{2k} \gamma_k \Phi_k^\dagger \mathbf{S}_{r,k} \Phi_k \mathbf{S}_{t,k} \right) \\ \text{s.t. } & |[\Phi_k]_{n,n}| = 1 \quad \forall k, n.\end{aligned}$$

- When the AS at each k -th RIS is very high ($\mathbf{S}_{t,k}$ and $\mathbf{S}_{r,k}$ essentially proportional to the unit matrix), the optimization over Φ_k 's is immaterial, since $\Sigma_k \approx \Phi_k^\dagger \Phi_k = \mathbf{I}_{N_s}$.

A. L. Moustakas, G. C. Alexandropoulos, and M. Debbah, "Reconfigurable intelligent surfaces and capacity optimization: A large system analysis," *IEEE TWC*, 2023.

Closed-Form Solution for Φ_k 's (2/3)

- When the AS is very small, so that $\mathbf{S}_{t,k}$ and $\mathbf{S}_{r,k}$ are unit-rank matrices (i.e., two LOS channels), it holds $\forall a, b$ that:
 $[\mathbf{S}_{r,k}]_{a,b} \approx N_s [\mathbf{u}_{rk,1} \mathbf{u}_{rk,1}^\dagger]_{a,b} = e^{i\mathbf{q}_{rk,1}^T(\mathbf{x}_a - \mathbf{x}_b)}$ and
 $[\mathbf{S}_{t,k}]_{a,b} \approx N_s [\mathbf{u}_{tk,1} \mathbf{u}_{tk,1}^\dagger]_{a,b} = e^{i\mathbf{q}_{tk,1}^T(\mathbf{x}_a - \mathbf{x}_b)}$; the wavevectors $\mathbf{q}_{tk,1}$ and $\mathbf{q}_{rk,1}$ correspond to the projection on the surface of each k -th RIS of the mean AoA/AoD of the EM wave's energy.
- In this case, $\boldsymbol{\Sigma}_k = N_s |\kappa_{k,11}|^2 \mathbf{u}_{rk,1} \mathbf{u}_{rk,1}^\dagger$ with
 $\kappa_{k,11} = \mathbf{u}_{rk,1}^\dagger \boldsymbol{\Phi}_k \mathbf{u}_{tk,1} = \frac{1}{N_s} \sum_{n=1}^{N_s} e^{i\phi_{k,n}} e^{-i(\mathbf{q}_{tk,1} - \mathbf{q}_{rk,1})^T \mathbf{x}_n}$.
- Hence, the $\boldsymbol{\Phi}_k$'s maximizing the ergodic MI are such that $\forall k, n$:

$$\phi_{k,n} = (\mathbf{q}_{tk,1} - \mathbf{q}_{rk,1})^T \mathbf{x}_n.$$

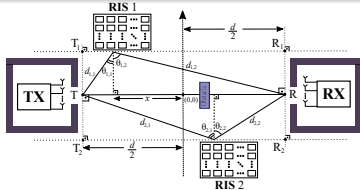
A. L. Moustakas, G. C. Alexandropoulos, and M. Debbah, "Reconfigurable intelligent surfaces and capacity optimization: A large system analysis," *IEEE TWC*, 2023.

Closed-Form Solution for Φ_k 's (3/3)

- Clearly, when the components of the incoming and outgoing direction vectors parallel to each k -th RIS are equal (i.e., $\mathbf{q}_{tk,1} = \mathbf{q}_{rk,1}$), which is the case of geometrical optics, no phase optimization is necessary.
- When the eigenvalue distributions of $\mathbf{S}_{r,k}$'s and $\mathbf{S}_{t,k}$'s are a displacement of one another in the domain space of \mathbf{q} , the differences of the \mathbf{q} -vectors of the corresponding eigenvalues in each distribution are constant and equal to the difference between the \mathbf{q} -vectors of the maximum eigenvalues of the matrices, i.e., $\mathbf{q}_{tk,\ell} - \mathbf{q}_{rk,\ell} = \mathbf{q}_{tk,1} - \mathbf{q}_{rk,1} \forall \ell \neq 1$. In this case, the proposed closed-form expression is optimal.
- If the domain of non-negligible eigenvalues of each $\mathbf{S}_{t,k}$ and $\mathbf{S}_{r,k}$ are not related by a shift in \mathbf{q} , then, the proposed closed-form expression may not be optimal, but will be close, and thus, can serve as an initial condition for further optimization.

A. L. Moustakas, G. C. Alexandropoulos, and M. Debbah, "Reconfigurable intelligent surfaces and capacity optimization: A large system analysis," *IEEE TWC*, 2023.

Closed-Form Solution for $d_{k,1}$ and $d_{k,2}$



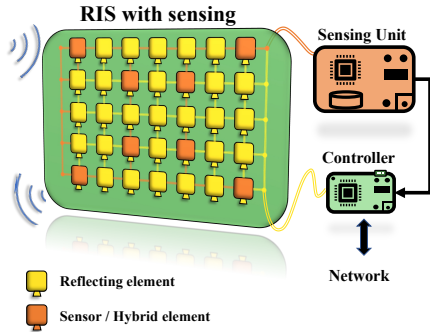
- The SNR due to the 1-st RIS, γ_1 , and its 2D Cartesian coordinate system, is maximized when the RIS is placed in the midpoint of the line segment T_1R_1 (i.e., at the $(0, h)$ point with $|h|$ being the length of the line segment T_1T) when $h \geq \frac{d}{2}$, or at the points $(\pm\sqrt{\frac{d^2}{4} - h^2}, h)$ when $h < \frac{d}{2}$.
- When possible ($h \rightarrow 0$), each RIS should be placed close to the TX or RX antenna arrays, playing the role of a reflector (i.e., holographic MIMO).

A. L. Moustakas, G. C. Alexandropoulos, and M. Debbah, "Reconfigurable intelligent surfaces and capacity optimization: A large system analysis," *IEEE TWC*, 2023.

T. Gong, P. Gavrilidis, R. Ji, C. Huang, G. C. Alexandropoulos, L. Wei, Z. Zhang, M. Debbah, H. V. Poor, and C. Yuen, "Holographic MIMO 6G communications: Theoretical foundations, enabling technologies, and future directions," *IEEE Commun. Surveys & Tuts.*, 2024.

N. Shlezinger, G. C. Alexandropoulos, M. F. Imani, Y. C. Eldar, and D. R. Smith, "Dynamic metasurface antennas for 6G extreme massive MIMO communications," *IEEE WCOM*, 2021. (**IEEE ComSoc Fred Ellersick Prize 2024**)

Individual Channel Estimation with Hybrid RISs



A. Masaracchia, D. V. Huynh, G. C. Alexandropoulos, B. Canberk, O. A. Dobre, and T. Q. Duong, "Towards the metaverse realization in 6G: Orchestration of RIS-enabled smart wireless environments via digital twins," *IEEE IoT Mag.*, 2024.

G. C. Alexandropoulos and E. Vlachos, "A hardware architecture for reconfigurable intelligent surfaces with minimal active elements for explicit channel estimation," *Proc. IEEE ICASSP*, 2020.

I. Alamzadeh, G. C. Alexandropoulos, N. Shlezinger, and M. F. Imani, "A reconfigurable intelligent surface with integrated sensing capability," *Scientific Reports*, 2021.

G. C. Alexandropoulos, N. Shlezinger, I. Alamzadeh, M. F. Imani, H. Zhang, and Y. C. Eldar, "Hybrid reconfigurable intelligent metasurfaces: Enabling simultaneous tunable reflections and sensing for 6G wireless communications," *IEEE VTM*, 2024.

MI Performance vs. Angular Spread

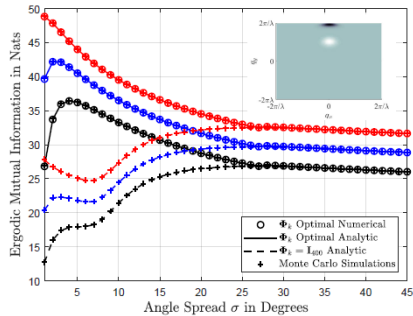


Fig. 3. The ergodic MI performance in nats per channel use for $N_t = 8$, $N_r = 4$, and $\rho = 10$ dB versus the AS σ in degrees, for a system operating at 2.5 GHz with $K = 1$ (black), $K = 2$ (blue), and $K = 4$ (red) RISs present. Each RIS is a square lattice of 20×20 reflecting elements of inter-element distance $\lambda/2 = 6$ cm, and the case where there is no direct link between TX and RX has been considered. As depicted, RIS optimization plays a prominent role in low AS values for the simulated large $N_s = 400$ value (i.e., correlated channels), while for large ASs, the RIS optimization becomes unnecessary. The inset figure depicts the distribution of the eigenvalues of the incoming (white ellipsis) and outgoing (black ellipsis) EM waves with incoming angle $\theta_1 = 30^\circ$ and outgoing angle $\theta_2 = 70^\circ$, respectively, as well as AS value $\sigma = 5^\circ$.

A. L. Moustakas, G. C. Alexandropoulos, and M. Debbah, "Reconfigurable intelligent surfaces and capacity optimization: A large system analysis," *IEEE TWC*, 2023.

MI Performance vs. Incident Angle

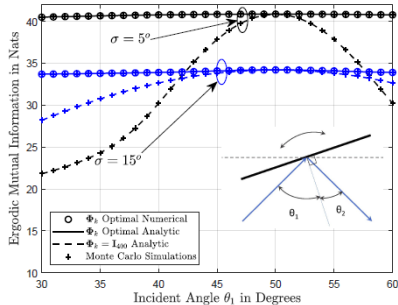


Fig. 4. The ergodic MI performance in nats per channel use in the presence of $K = 2$ RISs as a function of the mean incoming angle θ_1 in degrees (essentially as a function of the degree of tilting the RISs), considering the two different values $\sigma = 5^\circ$ and 15° of the incoming and outgoing EM waves' ASs. The RISs are equidistant from the TX and RX antennas, with the total mean incident and outgoing angles satisfying the relationship $\theta_{tot} = \theta_1 + \theta_2 = 100^\circ$, and are tilted with respect to the horizontal axis, as shown in the inset figure. The rest of the system parameters are the same with Fig. 3. The figure showcases that, in the low AS case for fixed phase configurations $\Phi_k = \bar{\Phi}_{400}$ for $k = 1$ and 2, the maximum MI is achieved when $\theta_1 = \theta_2$ (i.e., geometrical optics). This maximum performance is also obtained by the proposed analytical optimization as well as the considered numerical one. In fact, it is also depicted that, when the RISs are optimized (analytically or numerically), the MI has approximately the same maximum value, irrespective of the lattice orientation.

A. L. Moustakas, G. C. Alexandropoulos, and M. Debbah, "Reconfigurable intelligent surfaces and capacity optimization: A large system analysis," *IEEE TWC*, 2023.

MI Performance vs. Number of RIS Elements

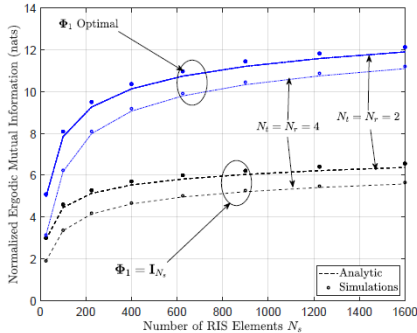


Fig. 5. The ergodic MI performance in nats per channel use per TX antenna for the case of a single (i.e., $K = 1$) square-shaped RIS, as a function of the number N_s of its reflecting elements. A communication channel with AS equal to $\sigma = 5^\circ$, central frequency 2.5 GHz and inter-RIS-element distance $\lambda/2 = 6$ cm, and $\rho = 10$ dB operating SNR, are considered. As in Fig. 3, the mean incoming and outgoing angles are set to $\theta_1 = 30^\circ$ and $\theta_2 = 70^\circ$, respectively. The figure includes curves with the analytically optimized phase configuration, as well as the unoptimized case, considering the settings $N_t = N_r = \{2, 4\}$ for the number of TX and RX antennas. It is demonstrated that the analytically obtained values are quite close with equivalent simulations, thus, validating our analysis even for small numbers of N_s , N_t , and N_r , and that the relative gain of RIS optimization decreases with increasing N_s values.

A. L. Moustakas, G. C. Alexandropoulos, and M. Debbah, "Reconfigurable intelligent surfaces and capacity optimization: A large system analysis," *IEEE TWC*, 2023.

MI Performance vs. Horizontal Distance

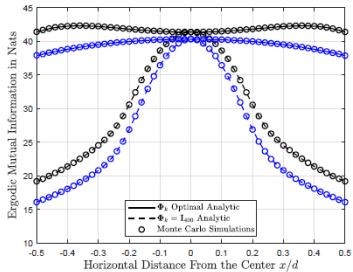
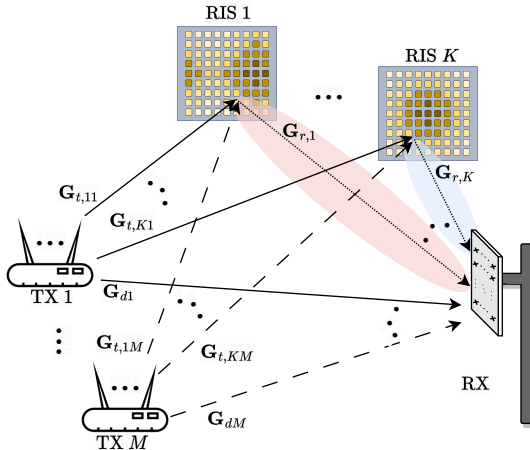


Fig. 6. The ergodic MI performance in nats per channel use, when $K = 2$ RISs are present, as a function of the normalized horizontal distance x/d (unitless) between the TX and RX antenna arrays measured from the origin in Fig. 1. The SNR between the latter end nodes varies with the horizontal distance x as shown in (3) for $h = 0.7d$ (blue curves) and with $h = 0.3d$ (black curves). The actual variation of the SNR with x for these two cases is shown in the following Fig. 7. The dashed curves represent the case where $\Phi_k = \mathbf{I}_{400}$ for $k = 1$ and 2, while the solid curves correspond to the case where Φ_k 's are optimized using the analytical expression (25), for the corresponding mean angles of arrival and departure that are mapped to the specific location of the RISs (see Fig. 1). In the case of $h = 0.7d$ (blue), for which the SNR is maximum at the center, the MI gets clearly its maximum value at this point $x = 0$. In contrast, in the case of $h = 0.3d$, for which the SNR becomes maximum away from the center (see the inset figure and Proposition 3), the maximum MI appears at the point where the SNR is maximized. Nevertheless, it is evident that the optimization of the RIS makes the MI remain nearly constant as a function of distance, despite the variations of both the SNR and the angles of arrival and departure of the incoming and outgoing EM waves, respectively, at the RISs.

A. L. Moustakas, G. C. Alexandropoulos, and M. Debbah, "Reconfigurable intelligent surfaces and capacity optimization: A large system analysis," *IEEE TWC*, 2023.

The MIMO-MAC-RIS Channel



A. L. Moustakas and G. C. Alexandropoulos, "MIMO MAC empowered by reconfigurable intelligent surfaces: Capacity region and large system analysis," *IEEE TWC*, 2024.

The MIMO-MAC-RIS Channel and Capacity Region

- Received signal: $\mathbf{y} \triangleq \sum_{m=1}^M \mathbf{G}_{\text{tot},m} (\{\Phi_k\}_{k=1}^K) \mathbf{x}_m + \mathbf{z}$ with $\mathbf{G}_{\text{tot},m} (\{\Phi_k\}_{k=1}^K) \triangleq \mathbf{G}_{dm} + \sum_{k=1}^K \mathbf{G}_{r,k} \Phi_k \mathbf{G}_{t,km}$ and $\mathbf{Q}_m \triangleq \mathbb{E}[\mathbf{x}_m \mathbf{x}_m^\dagger]$.
- The MIMO-MAC-RIS capacity region consists of all rate multiplets $\{R_1, R_2, \dots, R_M\}$ such that it holds for all sets $\mathcal{S} \subseteq \{1, 2, \dots, M\}$ with $\text{Tr}\{\mathbf{Q}_m\} \leq N_t \forall m$:

$$\sum_{m \in \mathcal{S}} R_m \leq \mathbb{E} \left[\log \det \left(\mathbf{I}_{N_r} + \underbrace{\sum_{m \in \mathcal{S}} \mathbf{G}_{\text{tot},m} (\{\Phi_k\}_{k=1}^K) \mathbf{Q}_m \mathbf{G}_{\text{tot},m}^\dagger (\{\Phi_k\}_{k=1}^K)}_{\triangleq I(\{\mathbf{Q}_m\}_{m \in \mathcal{S}}, \{\Phi_k\}_{k=1}^K)} \right) \right].$$

- \mathbf{Q}_m 's and Φ_k 's corresponding to the borders of this region are obtained by maximizing ($\boldsymbol{\mu} \triangleq [\mu_1, \mu_2, \dots, \mu_M]$, $\mu_1 \geq \mu_2 \geq \dots \geq \mu_M$, and $\sum_{\ell=1}^M \mu_\ell = 1$):

$$L_M (\{\mathbf{Q}_m\}_{m=1}^M, \{\Phi_k\}_{k=1}^K, \boldsymbol{\mu}) \triangleq \mu_M I (\{\mathbf{Q}_m\}_{m=1}^M, \{\Phi_k\}_{k=1}^K)$$

$$+ \sum_{\ell=1}^{M-1} (\mu_\ell - \mu_{\ell+1}) I (\{\mathbf{Q}_m\}_{m=1}^\ell, \{\Phi_k\}_{k=1}^K).$$

A. L. Moustakas and G. C. Alexandropoulos, "MIMO MAC empowered by reconfigurable intelligent surfaces: Capacity region and large system analysis," *IEEE TWC*, 2024.

Closed-Form Ergodic Sum-MI Formula

- In the limit $N_t, N_r, N_s \rightarrow \infty$ with fixed ratios $\beta_r \triangleq N_r/N_t$ and $\beta_s \triangleq N_s/N_t$, the ergodic MI per TX antenna element takes the closed form:

$$\begin{aligned} C_M \left(\{\mathbf{Q}_m\}_{m=1}^M, \{\Phi_k\}_{k=1}^K \right) &= \frac{1}{N_t} \log \det \left(\mathbf{I}_{N_r} + \tilde{\mathbf{R}} \right) \\ &+ \frac{1}{N_t} \sum_{k=1}^K \sum_{m=1}^M \log \det \left(\mathbf{I}_{N_s} + t_{1k} r_{2km} \boldsymbol{\Sigma}_{km} \right) + \frac{1}{N_t} \sum_{m=1}^M \log \det \left(\mathbf{I}_{N_t} + \mathbf{Q}_m \tilde{\mathbf{T}}_m \right) \\ &- \sum_{m=1}^M \left(r_{dm} t_{dm} + \sum_{k=1}^K (r_{1km} t_{1k} + r_{2km} t_{2km}) \right). \end{aligned}$$

where the parameters t_{dm} , t_{2km} , r_{dm} , r_{2km} , r_{1km} , and t_{1k} are the unique solutions of some fixed point equations and:

$$\begin{aligned} \tilde{\mathbf{R}} &\triangleq \sum_{m=1}^M \left(r_{dm} \mathbf{R}_{dm} + \sum_{k=1}^K r_{1km} \mathbf{R}_k \right), \quad \tilde{\mathbf{T}} \triangleq t_{dm} \mathbf{T}_{dm} + \sum_{k=1}^K t_{2km} \mathbf{T}_{km}, \\ \boldsymbol{\Sigma}_{km} &\triangleq \mathbf{S}_{t,km}^{1/2} \Phi_k^\dagger \mathbf{S}_{r,k} \Phi_k \mathbf{S}_{t,km}^{1/2}. \end{aligned}$$

A. L. Moustakas, G. C. Alexandropoulos, and M. Debbah, "Reconfigurable intelligent surfaces and capacity optimization: A large system analysis," *IEEE TWC*, 2023.

Optimization of the Asymptotic Ergodic Sum MI

- The boundaries of the ergodic MIMO-MAC capacity region in the presence of multiple RISs:

$$\mathcal{OP}_3 : \max_{\{\Phi_k\}_{k=1}^K} \left[\mu_M C_M (\{\Phi_k\}_{k=1}^K) + \sum_{\ell=1}^{M-1} (\mu_\ell - \mu_{\ell+1}) C_\ell (\{\Phi_k\}_{k=1}^K) \right]$$

s.t. $|[\Phi_k]_{n,n}| = 1 \quad \forall k, n.$

- Using the previously derived asymptotic formula, we now focus on the optimization problem:

$$\mathcal{OP}_4 : \max_{\Phi_k} \sum_{m=1}^M \log \det \left(\mathbf{I}_{N_s} + t_{1k} r_{2km} \Phi_k^\dagger \mathbf{S}_{r,k} \Phi_k \mathbf{S}_{t,km} \right)$$

s.t. $|[\Phi_k]_{n,n}| = 1 \quad \forall k, n.$

A. L. Moustakas and G. C. Alexandropoulos, "MIMO MAC empowered by reconfigurable intelligent surfaces: Capacity region and large system analysis," *IEEE TWC*, 2024.

The Vanishing Angle Spread Case (1/2)

- Let $\mathbf{S}_{t,m} = N_s \mathbf{u}_m \mathbf{u}_m^\dagger \forall m$ and $\mathbf{S}_r = N_s \mathbf{v} \mathbf{v}^\dagger$ be of unit rank.
- The unit-norm vectors \mathbf{u}_m and \mathbf{v} correspond to the wave vectors of the incoming signal from the m -th TX and the outgoing signal to the RX:

$$[\mathbf{u}_m]_n = \frac{1}{\sqrt{N_s}} e^{i \mathbf{q}_{t,m} \mathbf{x}_n}, \quad [\mathbf{v}]_n = \frac{1}{\sqrt{N_s}} e^{i \mathbf{q}_r \mathbf{x}_n},$$

where $\mathbf{q}_{t,m}$ and \mathbf{q}_r are the incoming wave-vectors from the m -th TX to the RIS and the outgoing wave vector from the RIS to the RX, respectively.

- To this end, \mathcal{OP}_4 's objective for one RIS (Φ) becomes ($\Delta \mathbf{q}_m \triangleq \mathbf{q}_r - \mathbf{q}_{tm}$):

$$D_M(\Phi) \triangleq \sum_{m=1}^M \log \left(1 + N_s^2 t_{1m} r_{2m} \underbrace{\left| \frac{1}{N_s} \sum_{n=1}^{N_s} e^{i(\phi_n - \Delta \mathbf{q}_m \mathbf{x}_n)} \right|^2}_{\triangleq \kappa_m(\Phi)} \right).$$

- When $M = 1$ TX, yields $\phi_n = \Delta \mathbf{q} \mathbf{x}_n \forall n$.

A. L. Moustakas and G. C. Alexandropoulos, "MIMO MAC empowered by reconfigurable intelligent surfaces: Capacity region and large system analysis," *IEEE TWC*, 2024.

The Vanishing Angle Spread Case (2/2)

- When $M > 1$ TXs, each of the phase components ϕ_n needs to be chosen to optimize all $\kappa_m(\Phi)$'s simultaneously: *the more separated the quantities $\Delta\mathbf{q}_m$'s for different values of m are, the higher the competition of the terms in the summation, and hence, the smaller the values of $D_M(\Phi)$ will be.*
- \mathcal{OP}_4 with $D_M(\Phi)$ as its objective can be iteratively optimized as (ϵ is a convergence parameter):

$$\phi_n^{(i)} = \phi_n^{(i-1)} + \epsilon \sum_{m=1}^M \operatorname{Im} \left(\frac{N_s t_{1m} r_{2m} \kappa_m \left(\Phi^{(i-1)} \right) e^{i \left(\Delta\mathbf{q}_m \mathbf{x}_n - \phi_n^{(i-1)} \right)}}{1 + N_s^2 t_{1m} r_{2m} \left| \kappa_m \left(\Phi^{(i-1)} \right) \right|^2} \right) \quad \forall n.$$

The General Case

- In this case, the full gradient of the functional objective appearing in \mathcal{OP}_4 with respect to each of the RIS phase configuration matrices needs to be computed, yielding the iterations:

$$\phi_n^{(i)} = \phi_n^{(i-1)} + \epsilon \sum_{m=1}^M \text{Im} \left[\left(\mathbf{I}_{N_s} + t_{1m} r_{2m} \left(\boldsymbol{\Phi}^{(i-1)} \right)^\dagger \mathbf{S}_r \boldsymbol{\Phi}^{(i-1)} \mathbf{S}_{t,m} \right)^{-1} \right]_{n,n} \quad \forall n.$$

A. L. Moustakas and G. C. Alexandropoulos, "MIMO MAC empowered by reconfigurable intelligent surfaces: Capacity region and large system analysis," *IEEE TWC*, 2024.

Sum-MI Performance vs. Angular Spread

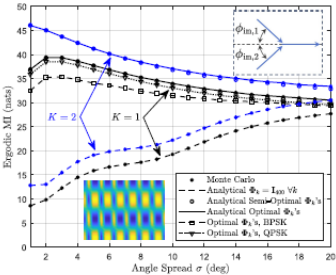


Fig. 2. The ergodic sum-MI performance in nats per channel use for $M = 2$ TXs and for $K = 1$ and 2 RISs versus the angle spread σ in degrees. All parameter values of this simulation setup appear in Table I, except for the incoming signal azimuth angles from each TX to the RISs, which are set as $\phi_{in,1} = 45^\circ$ and $\phi_{in,2} = -45^\circ$, as can be seen in the upper inset. In the case of two RISs, we have kept for simplicity the same parameter values, essentially locating the second RIS at the mirrored location of the first with respect to the plane of the TXs and the RX. The “o” points correspond to the Φ_k ’s obtained using the algorithm of Section IV-A, while the solid curves correspond to the optimized Φ_k ’s presented in Section IV-B. We see that they practically coincide with each other and with the Monte Carlo simulations. It is also depicted that the benefit of having two RISs (blue curves) serving both TXs is relatively minor, at least as compared with the large performance increase of the presence of one RIS compared to none (dashed curves). We have also added two curves depicting the ergodic sum MI for the case of a single RIS where its phases are 1-bit quantized to BPSK values (i.e., $e^{j\phi} = \pm 1$) and 2-bit quantized QPSK values (i.e., $e^{j\phi} = (\pm 1 \pm i)/\sqrt{2}$). It is shown that, in both cases, the optimization gain is significant, with the QPSK case being practically identical to the fully optimal case. Similar behavior had been obtained when two RISs are present, but we have not included the curves so as not to clutter the figure. Finally, the lower inset figure depicts the optimal phase distribution on the RIS for the continuous case when the angle spread is equal to $\sigma = 5^\circ$.

A. L. Moustakas and G. C. Alexandropoulos, “MIMO MAC empowered by reconfigurable intelligent surfaces: Capacity region and large system analysis,” *IEEE TWC*, 2024.

Sum-MI Performance vs. Incoming Signals' Angles

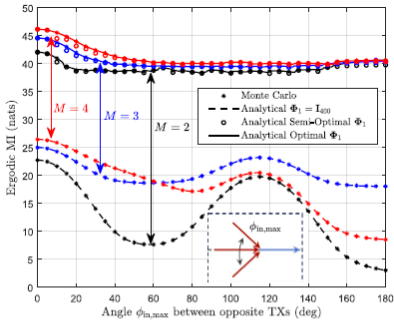


Fig. 3. The ergodic sum-capacity performance in nats per channel use in the presence of $K = 1$ RIS for $M = 2$ (black), 3 (blue), and 4 (red) TXs. All incoming and outgoing signals were considered to have angle spread $\sigma = 4^\circ$. The remaining simulation parameters take values from Table I. For the cases where $M > 1$, the TXs have incoming azimuth angles that are equidistant with maximum angle equal to the one plotted on the x-axis of the plot. For concreteness, we have included an inset which shows the azimuth angles for the case of $M = 3$. The solid lines correspond to the optimized Φ_1 , while the dashed ones correspond to the semi-optimal approach described in Section IV-A. The dotted lines correspond to Monte Carlo simulations, while the lower curves depict the sum-MI without any optimization, i.e., for $\Phi_1 = \mathbf{I}_{400}$. It is evident that, for increasing M , the relative gain is diminishing. Also, for increasing azimuth distance between TXs, it is demonstrated that the capacity gains are decreasing. This happens because the optimum Φ_1 has difficulties satisfying all TXs effectively.

A. L. Moustakas and G. C. Alexandropoulos, "MIMO MAC empowered by reconfigurable intelligent surfaces: Capacity region and large system analysis," *IEEE TWC*, 2024.

Capacity Region vs. Angular Spread

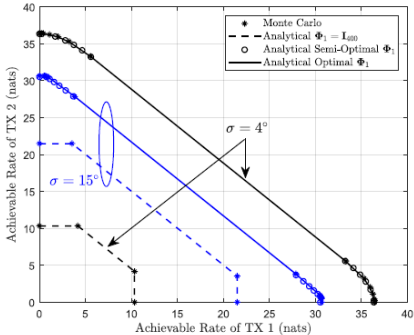
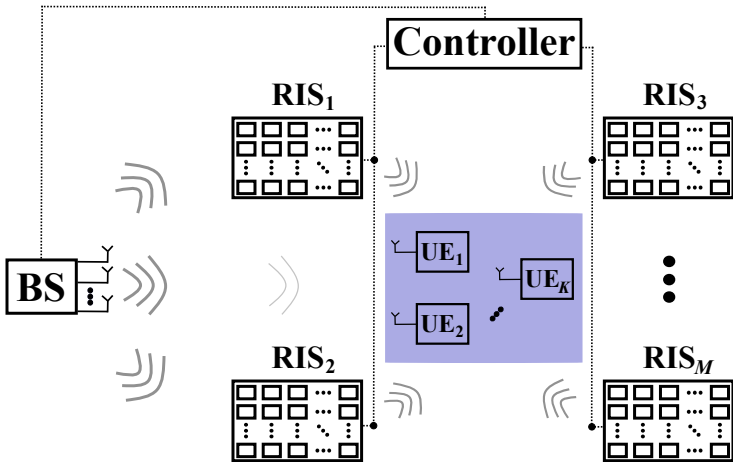


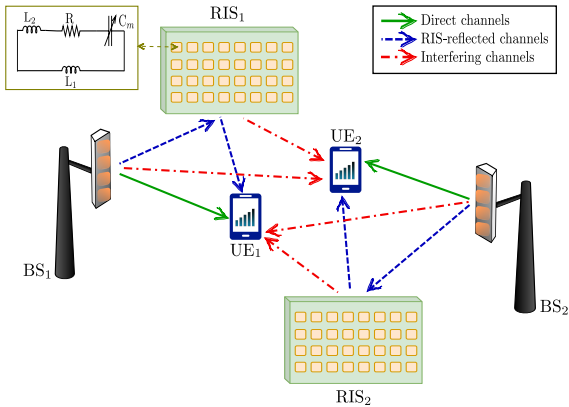
Fig. 4. Ergodic capacity region for the case of $M = 2$ TXs and $K = 1$ RIS, with incoming signal azimuth angles from each TX set to $\phi_{\text{in},1} = 45^\circ$ and $\phi_{\text{in},2} = -45^\circ$, considering the angle spread values $\sigma = 4^\circ$ (black) and $\sigma = 15^\circ$ (blue). All other parameter values are included in Table I. The upper two curves correspond to the capacity region boundary obtained by optimizing Φ_1 for $0 \leq \mu_1 \leq 1$ and $\mu_2 = 1 - \mu_1$ in (23). It is clear that (especially for $\sigma = 4^\circ$) the boundary is not a pentagon, in contrast to the lower two curves for which $\Phi_1 = \mathbf{I}_{400}$. The fact that the lower angle spread has a wider capacity region can be expected from Fig. 2. The solid curves correspond to the optimal capacity region boundaries calculated using the full optimization approach of Section IV-B. Finally, the rate pairs evaluated from Monte Carlo simulations using the Φ_1 obtained by numerically optimizing expression (9) for $\mu_1 = 0 : 0.1 : 1$ and $\mu_2 = 1 - \mu_1$ are illustrated.

Multi-RIS-Empowered Broadcast Channel



G. C. Alexandropoulos, K. Stylianopoulos, C. Huang, C. Yuen, M. Bennis, and M. Debbah, "Pervasive machine learning for smart radio environments enabled by reconfigurable intelligent surfaces," *Proc. IEEE*, 2022.

Multi-RIS-Empowered Interference (Broadcast) Channel



K. D. Katsanos, P. Di Lorenzo, and G. C. Alexandropoulos, "Multi-RIS-empowered multiple access: A distributed sum-rate maximization approach," *IEEE JSTSP*, 2024.

K. D. Katsanos, P. Di Lorenzo, and G. C. Alexandropoulos, "The interference broadcast channel with reconfigurable intelligent surfaces: A cooperative sum-rate maximization approach," *Proc. IEEE SPAWC*, 2024.

K. Katsanos and G. C. Alexandropoulos, "Robust consensus-based distributed beamforming for wideband cell-free multi-RIS MISO systems," *Proc. Asilomar*, 2025.

RIS Element Frequency Response

- Let the equivalent resonant circuit of each m -th ($m = 1, 2, \dots, M$) unit element each q -th RIS ($q = 1, 2, \dots, Q$) comprise a resistor R , a tunable capacitor C_{mq} , and two inductors L_1 and L_2 .
- The frequency response of each m -th unit element of each q -th RIS is modeled as:

$$\phi_{mq}(f, C_{mq}) \triangleq \frac{\mathcal{Z}(f, C_{mq}) - \mathcal{Z}_0}{\mathcal{Z}(f, C_{mq}) + \mathcal{Z}_0},$$

where \mathcal{Z}_0 is the free space impedance and

$$\mathcal{Z}(f, C_{mq}) \triangleq \frac{j2\pi f L_1 \left(j2\pi f L_2 + R + \frac{1}{j2\pi f C_{mq}} \right)}{j2\pi f (L_1 + L_2) + R + \frac{1}{j2\pi f C_{mq}}}.$$

K. D. Katsanos, N. Shlezinger, M. F. Imani, and G. C. Alexandropoulos, "Wideband multi-user MIMO communications with frequency selective RISs: Element response modeling and sum-rate maximization," *Proc. IEEE ICC*, 2022.

Received Signal Model

- The baseband received signal at each q -th single-antenna UE at each k -th subcarrier:

$$y_{qk} \triangleq \mathbf{f}_{qq,k}^H \mathbf{w}_{qk} x_{qk} + \sum_{j \neq q}^Q \mathbf{f}_{jq,k}^H \mathbf{v} w_{jk} x_{jk} + n_{qk},$$
$$\mathbf{f}_{qq,k}^H \triangleq \mathbf{h}_{qq,k}^H + \mathbf{g}_{qq,k}^H \mathbf{S}_q \boldsymbol{\Phi}_{qk} \mathbf{H}_{qq,k},$$
$$\mathbf{f}_{jq,k}^H \triangleq \mathbf{h}_{jq,k}^H + \mathbf{g}_{jq,k}^H \mathbf{S}_j \boldsymbol{\Phi}_{jk} \mathbf{H}_{jj,k}.$$

- Each $\mathbf{h}_{jq,k} \in \mathbb{C}^{N \times 1}$ ($q, j = 1, 2, \dots, Q$) indicates the direct channel between the q -th UE and the j -th BS at each k -th subcarrier.
- $\mathbf{H}_{qq,k}$ and $\mathbf{g}_{qq,k}$ denote each q -th BS-RIS and each q -th RIS-UE channel, respectively, at each k -th subcarrier.

- The achievable sum-rate performance for each q -th BS-RIS-UE link:

$$\mathcal{R}_q \left(\tilde{\mathbf{w}}, \tilde{\mathbf{c}}, \tilde{\mathbf{S}} \right) = \sum_{k=1}^K \log_2 \left(1 + \frac{|\mathbf{f}_{qq,k}^H \mathbf{w}_{qk}|^2}{\sigma_q^2 + \sum_{j \neq q}^Q |\mathbf{f}_{jq,k}^H \mathbf{w}_{jk}|^2} \right),$$

- i) $\tilde{\mathbf{w}} \triangleq [\mathbf{w}_1^T, \mathbf{w}_2^T, \dots, \mathbf{w}_Q^T]^T$ captures the linear precoding vector;
- ii) $\tilde{\mathbf{c}} \triangleq [\mathbf{c}_1^T, \mathbf{c}_2^T, \dots, \mathbf{c}_Q^T]^T$, with $\mathbf{c}_q \triangleq [C_{1q}, C_{2q}, \dots, C_{Mq}]^T$, denotes the tunable capacitances of each q -th RIS; and
- iii) $\tilde{\mathbf{S}} \triangleq \{\mathbf{S}_q\}_{q=1}^Q$ is the set of switch selection matrices at the Q beyond-diagonal RISs.

Problem Formulation

- Consider the following design optimization problem:

$$\begin{aligned} \mathcal{OP}_5 : \max_{\widetilde{\mathbf{w}}, \widetilde{\mathbf{c}}, \widetilde{\mathbf{S}}} \quad & \sum_{q=1}^Q \mathcal{R}_q \left(\widetilde{\mathbf{w}}, \widetilde{\mathbf{c}}, \widetilde{\mathbf{S}} \right) \\ \text{s.t.} \quad & \sum_{k=1}^K \|\mathbf{w}_{qk}\|^2 \leq P_q, \quad \mathbf{S}_q \in \mathcal{S}, \quad \forall q = 1, 2, \dots, Q, \\ & C_{\min} \leq [\mathbf{c}_q]_m \leq C_{\max}, \quad \forall m = 1, 2, \dots, M. \end{aligned}$$

- $\mathcal{S} \triangleq \left\{ \mathbf{S} \in \{0, 1\}^{M \times M} : \mathbf{S}\mathbf{1} = \mathbf{1}, \mathbf{S}^T\mathbf{1} = \mathbf{1} \right\}$: feasible set for the switch selection matrices at the beyond-diagonal RISs.
- C_{\min} and C_{\max} : minimum and maximum allowable values for the RIS tunable capacitances.

Distributed \mathcal{OP} Solution (1/3)

- Assume that each q -th BS possesses the channel gain matrices (included in $\mathbf{f}_{qq,k}$).
- Re-writting \mathcal{OP}_5 's sum-rate objective ($\mathbf{X}_q \triangleq \{\mathbf{w}_q, \mathbf{c}_q, \mathbf{S}_q\}$ and \mathbf{X}_{-q} is the set of all other users' variables except the q -th one):

$$\overline{\mathcal{R}}(\mathbf{X}_q, \mathbf{X}_{-q}) \triangleq \mathcal{R}_q(\mathbf{X}_q, \mathbf{X}_{-q}) + \sum_{j \neq q}^Q \mathcal{R}_j(\mathbf{X}_q, \mathbf{X}_{-q}).$$

- The latter structure naturally leads to the following decomposition scheme at every iteration t :
 - ① $\mathcal{R}_q(\mathbf{X}_q, \mathbf{X}_{-q})$ can be replaced by a surrogate function, denoted as $\tilde{\mathcal{R}}_q(\mathbf{X}_q, \mathbf{X}^t)$, which depends on the current iterate \mathbf{X}^t .
 - ② $\sum_{j \neq q}^Q \mathcal{R}_j(\mathbf{X}_q, \mathbf{X}_{-q})$ can be linearized around \mathbf{X}_q^t .

K. D. Katsanos, P. Di Lorenzo, and G. C. Alexandropoulos, "Multi-RIS-empowered multiple access: A distributed sum-rate maximization approach," *IEEE JSTSP*, 2024.

Distributed \mathcal{OP} Solution (2/3)

- The local surrogate function ($\gamma_{\mathbf{c}_q}^t \triangleq \nabla_{\mathbf{c}_q} \mathcal{R}_q(\mathbf{x}_q, \mathbf{x}_{-q}^t)|_{\mathbf{c}_q=\mathbf{c}_q^t}$ and $\Gamma_{\mathbf{S}_q}^t \triangleq \nabla_{\mathbf{S}_q} \mathcal{R}_q(\mathbf{x}_q; \mathbf{x}^t)|_{\mathbf{S}_q=\mathbf{S}_q^t}$):

$$\begin{aligned}\widetilde{\mathcal{R}}_q(\mathbf{X}_q; \mathbf{X}^t) &\triangleq \sum_{k=1}^K \log_2 \left(1 + \frac{|\mathbf{f}_{qq,k}^H \mathbf{w}_{qk}|^2}{\sigma_q^2 + \sum_{j \neq q} |\mathbf{f}_{jq,k}^H \mathbf{w}_{jk}^t|^2} \right) \\ &\quad - \frac{\tau}{2} \left(\|\mathbf{w}_q - \mathbf{w}_q^t\|^2 + \|\mathbf{c}_q - \mathbf{c}_q^t\|^2 + \|\mathbf{S}_q - \mathbf{S}_q^t\|_F^2 \right) \\ &\quad + \langle \gamma_{\mathbf{c}_q}^t, \mathbf{c}_q - \mathbf{c}_q^t \rangle + \langle \Gamma_{\mathbf{S}_q}^t, \mathbf{S}_q - \mathbf{S}_q^t \rangle.\end{aligned}$$

- At every algorithmic iteration t , each user q solves the following surrogate optimization problem:

$$\mathcal{OP}_6 : \quad \widehat{\mathbf{X}}_q^t = \arg \max_{\mathbf{X}_q \in \mathcal{X}_q} \widetilde{\mathcal{R}}_q(\mathbf{X}_q; \mathbf{X}^t) + \langle \boldsymbol{\Pi}_q^t, \mathbf{X}_q - \mathbf{X}_q^t \rangle,$$

where \mathcal{X}_q denotes the feasible set combining all \mathcal{OP}_5 constraints.

K. D. Katsanos, P. Di Lorenzo, and G. C. Alexandropoulos, "Multi-RIS-empowered multiple access: A distributed sum-rate maximization approach," *IEEE JSTSP*, 2024.

- Before, in \mathcal{OP}_6 , $\boldsymbol{\Pi}_q^t$ is defined as follows:

$$\boldsymbol{\Pi}_q^t \triangleq \sum_{j \neq q}^Q \nabla_{\mathbf{X}_q} \mathcal{R}_j(\mathbf{X}_q, \mathbf{X}_{-q}) \Big|_{\mathbf{X}_q = \mathbf{X}_q^t}.$$

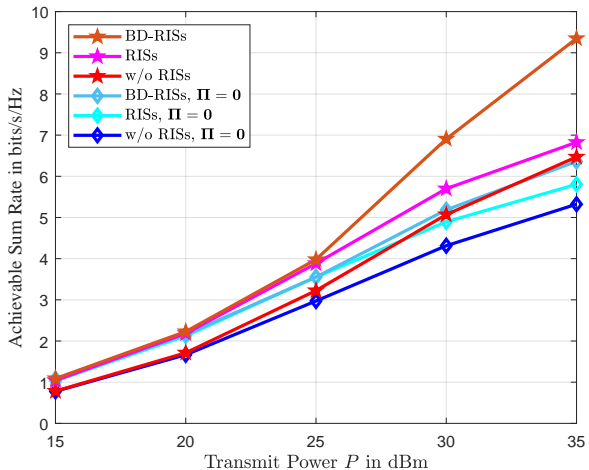
- The term $\nabla_{\mathbf{X}_q} \mathcal{R}_j(\mathbf{X}_q, \mathbf{X}_{-q}) \Big|_{\mathbf{X}_q = \mathbf{X}_q^t}$ is the *pricing vector*; it quantifies how the allocation of resources to user q affects the achievable rate of user j .
- The solution can be efficiently obtained with provable convergence to a KKT point.

Simulation Setup

- All nodes were considered positioned on a 3D Cartesian coordinate system.
- All wireless wideband channels were modeled as fading channels with D delay taps in the time-domain impulse response.
- For the fading component of each link, distance dependent pathloss was considered between any two nodes i and j with distance $d_{i,j}$ (where $i, j \in \{\text{BS}, \text{UE}, \text{RIS}\}$), modeled as $\text{PL}_{i,j} = \text{PL}_0(d_{i,j}/d_0)^{-\alpha_{i,j}}$ with $\text{PL}_0 = (\frac{\lambda_c}{4\pi})^2$.
- We have set equal BS's transmit power budget and noise variance for all users with $\sigma^2 = -90$ dBm.
- The carrier frequency is $f_c = 3.5$ GHz, the bandwidth $\text{BW} = 100$ MHz, and the number of subcarriers $K = 64$.

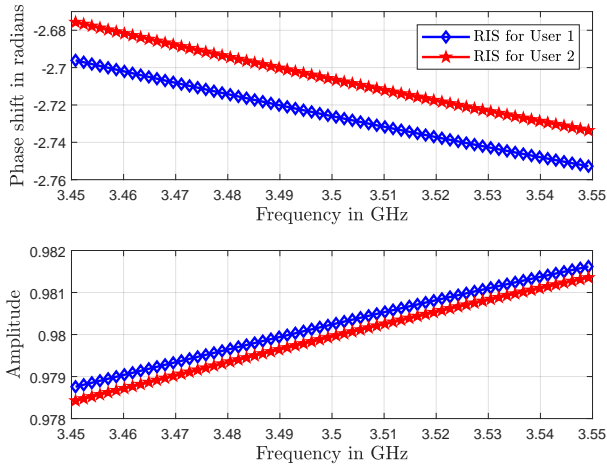
K. D. Katsanos, P. Di Lorenzo, and G. C. Alexandropoulos, "Multi-RIS-empowered multiple access: A distributed sum-rate maximization approach," *IEEE JSTSP*, 2024.

Achievable Sum-Rate vs. TX Power



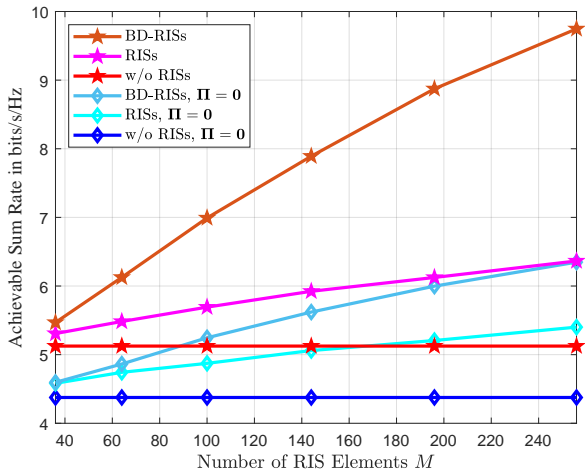
K. D. Katsanos, P. Di Lorenzo, and G. C. Alexandropoulos, "Multi-RIS-empowered multiple access: A distributed sum-rate maximization approach," *IEEE JSTSP*, 2024.

RIS Reflection Coefficient vs. Frequency



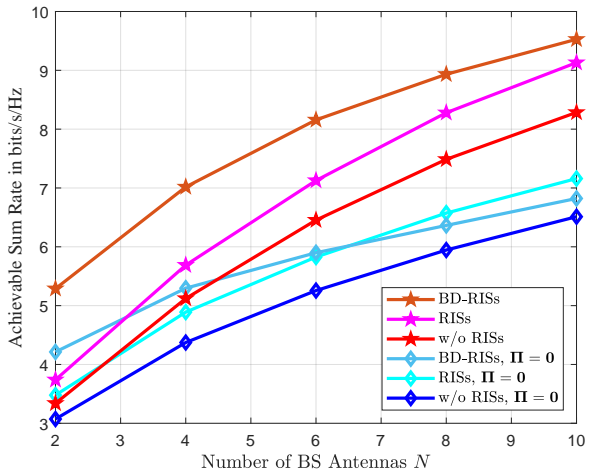
K. D. Katsanos, P. Di Lorenzo, and G. C. Alexandropoulos, "Multi-RIS-empowered multiple access: A distributed sum-rate maximization approach," *IEEE JSTSP*, 2024.

Achievable Sum-Rate vs. Number of RIS Elements



K. D. Katsanos, P. Di Lorenzo, and G. C. Alexandropoulos, "Multi-RIS-empowered multiple access: A distributed sum-rate maximization approach," *IEEE JSTSP*, 2024.

Achievable Sum-Rate vs. Number of BS Antennas



K. D. Katsanos, P. Di Lorenzo, and G. C. Alexandropoulos, "Multi-RIS-empowered multiple access: A distributed sum-rate maximization approach," *IEEE JSTSP*, 2024.

The Interference Broadcast Channel with Multiple RISs

- Received signal at each ℓ_q -th UE at each k -th subcarrier:

$$y_{\ell_q, k} = \mathbf{f}_{q, \ell_q, k}^H \mathbf{x}_{q, k} + \sum_{j \neq q}^Q \mathbf{f}_{j, \ell_q, k}^H \mathbf{x}_{j, k} + n_{\ell_q, k},$$

- Design objective:

$$\begin{aligned} & \max_{\widetilde{\mathbf{w}}, \widetilde{\mathbf{c}}, \widetilde{\mathbf{S}}} \quad \sum_{q=1}^Q \sum_{\ell=1}^{L_q} \mathcal{R}_{\ell_q} (\widetilde{\mathbf{w}}, \widetilde{\mathbf{c}}, \widetilde{\mathbf{S}}) \\ \text{s.t.} \quad & \sum_{\ell=1}^{L_q} \sum_{k=1}^K \|\mathbf{w}_{\ell_q, k}\|^2 \leq P_q, \mathbf{S}_q \in \mathcal{S}, \forall q = 1, \dots, Q, \\ & C_{\min} \leq [\mathbf{c}_q]_m \leq C_{\max}, \quad \forall m = 1, \dots, M. \end{aligned}$$

K. D. Katsanos, P. Di Lorenzo, and G. C. Alexandropoulos, "The interference broadcast channel with reconfigurable intelligent surfaces: A cooperative sum-rate maximization approach," *Proc. IEEE SPAWC*, 2024.

Achievable Sum-Rate vs. TX Power

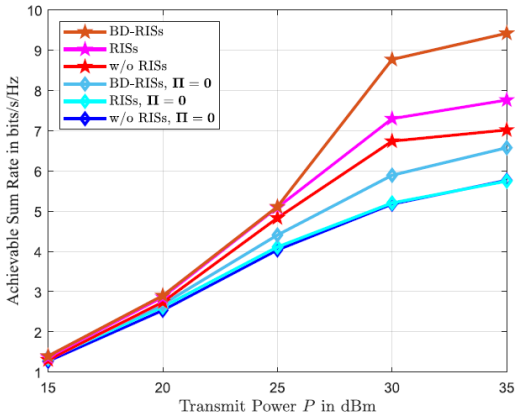


Fig. 1. Achievable sum-rate performance for $Q = 4$ BSs and RISs, each with $N = 4$ antennas and $M = 100$ unit elements, respectively.

K. D. Katsanos, P. Di Lorenzo, and G. C. Alexandropoulos, "The interference broadcast channel with reconfigurable intelligent surfaces: A cooperative sum-rate maximization approach," *Proc. IEEE SPAWC*, 2024.

The Cell-Free MISO Case with Shared RISs

- Received signal at each u -th UE at each k -th subcarrier:

$$y_{u,k} = \sum_{b=1}^B y_{b,u,k} + n_{u,k},$$
$$y_{b,u,k} = \left(\mathbf{h}_{b,u,k}^H + \sum_{r=1}^R \mathbf{g}_{r,u,k}^H \boldsymbol{\Phi}_{r,k} \mathbf{H}_{b,r,k} \right) \sum_{q=1}^U \mathbf{w}_{b,q,k} s_{q,k}.$$

- Design objective when only the CSI statistics are available:

$$\max_{\widetilde{\mathbf{w}}, \widetilde{\mathbf{c}}} \quad \mathcal{R} \triangleq \mathbb{E}_{\mathbf{h}, \mathbf{g}, \mathbf{H}} \left[\sum_{u=1}^U \mathcal{R}_u (\widetilde{\mathbf{w}}, \widetilde{\mathbf{c}}) \right]$$

$$\text{s.t.} \quad \sum_{u=1}^U \sum_{k=1}^K \|\mathbf{w}_{b,u,k}\|^2 \leq P_b^{\max} \quad \forall b \in \mathcal{B},$$

$$C_{\min} \leq [\mathbf{c}_r]_m \leq C_{\max} \quad \forall m \in \mathcal{M}.$$

K. Katsanos and G. C. Alexandropoulos, "Robust consensus-based distributed beamforming for wideband cell-free multi-RIS MISO systems," *Proc. Asilomar*, 2025.

The Role of Cooperation

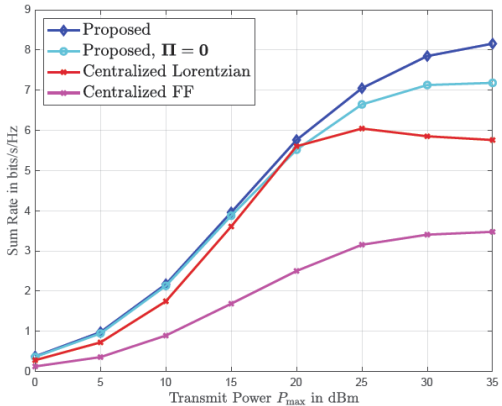


Fig. 1: Achievable sum-rate performance for the considered wideband cell-free MISO system with $B = 4$ BSs, each with $N = 2$ antennas, and $R = 2$ RISs with $M = 144$ unit elements each.

K. Katsanos and G. C. Alexandropoulos, "Robust consensus-based distributed beamforming for wideband cell-free multi-RIS MISO systems," *Proc. Asilomar*, 2025.

1 Part III: Distributed Sensing-Aided Communications

- Optimization of Multi-RIS-Aided Communications
- Distributed Learning for Multi-RIS-Aided Communications
- Position-Aided Near-Field Beam Tracking
- Sensing-Aided Communications via Hydrid RISs
- Over-the-Air Learning: The XL MIMO Potential

Multi-RIS-Empowered P2P Communications

- Received signal with K identical RISs:

$$y(t) = \mathbf{m}(t)\mathbf{v}(t)x(t) + \tilde{n}(t),$$

$$\mathbf{m}(t) \triangleq \mathbf{h}^H(t) + \sum_{k=1}^K \mathbf{h}_{2,k}^H(t) \boldsymbol{\Phi}_k(t) \mathbf{H}_{1,k}^H(t),$$

where $\mathbf{v}(t) \in \mathcal{V} \triangleq \{\mathbf{V}_{:,i}\}_{i=1}^{N_{\text{TX}}}$ with \mathbf{V} being the $N_{\text{TX}} \times N_{\text{TX}}$ DFT matrix and $\boldsymbol{\phi}_k(t) \triangleq [\phi_{1,k}(t), \phi_{2,k}(t), \dots, \phi_{N_{\text{RIS}},k}(t)]^T$ for each k -th RIS.

- Design problem definition:

$$\begin{aligned} \mathcal{OP}_7 : \max_{\{\boldsymbol{\phi}_k(t)\}_{k=1}^K, \mathbf{v}(t)} \quad & \gamma(t) \triangleq \frac{P}{\sigma^2} |\mathbf{m}(t)|^2 \\ \text{s.t.} \quad & \phi_{i,k}(t) \in \{\theta_1, \theta_2\} \quad \forall i, k, \quad \mathbf{v}(t) \in \mathcal{V}. \end{aligned}$$

G. Stamatelis, K. Stylianopoulos, and G. C. Alexandropoulos, "Evolving multi-branch attention convolutional neural networks for online RIS configuration," *IEEE TCCN*, 2025.

Main Challenge

- Perform channel estimation at each channel coherence time t and solve \mathcal{OP}_7 via iterative discrete optimization approaches (NP-hard); both need to be done on the order of few milliseconds.
- Let the following mapping:

$$\left\{ \left\{ \phi_k(t) \right\}_{k=1}^K, \mathbf{v}(t) \right\} = g \left(\mathbf{h}(t), \left\{ \mathbf{H}_{1,k}(t) \right\}_{k=1}^K, \left\{ \mathbf{h}_{2,k}(t) \right\}_{k=1}^K \right),$$

according to which the e2e SNR becomes:

$$\gamma \left(\left\{ \left\{ \phi_k(t) \right\}_{k=1}^K, \mathbf{v}(t) \right\} \right) = \gamma \left(g \left(\mathbf{h}(t), \left\{ \mathbf{H}_{1,k}(t) \right\}_{k=1}^K, \left\{ \mathbf{h}_{2,k}(t) \right\}_{k=1}^K \right) \right).$$

- This implies that the set \mathcal{G} of all applicable mappings $g(\cdot)$ may contain a function mapping the involved channels to the feasible sets of the RIS phase profiles and TX precoders; still impractical to find $g(\cdot)$ with per-time-instant optimization.

G. Stamatelis, K. Stylianopoulos, and G. C. Alexandropoulos, "Evolving multi-branch attention convolutional neural networks for online RIS configuration," *IEEE TCCN*, 2025.

Decision Making over Various Channels

- **Idea 1:** Relax \mathcal{OP}_7 and focus on finding a general mapping $g(\cdot)$ performing online near-optimal decisions for a wide variety of channel inputs.
- Consider a finite time horizon T and solve:

$$\begin{aligned}\mathcal{OP}_8 : \max_{g(\cdot) \in \mathcal{G}} \quad & \frac{1}{T} \mathbb{E} \left[\sum_{t=1}^T \gamma(g(\mathbf{h}(t), \{\mathbf{H}_{1,k}(t)\}_{k=1}^K, \{\mathbf{h}_{2,k}(t)\}_{k=1}^K)) \right] \\ \text{s.t. } & \phi_{i,k}(t) \in \{\theta_1, \theta_2\} \quad \forall i, k \text{ and } \mathbf{v}(t) \in \mathcal{V}.\end{aligned}$$

- Then, at every time instant t , collect the current CSI and replace it in the optimized $g(\cdot)$ to obtain the phase profiles of the K RISs and the TX precoder.
- **Idea 2:** Parameterize $g(\cdot)$ with an NN; optimize the NN weights offline via large numbers of user trajectories of length T , and then approximate the expectation via averaging.

G. Stamatelis, K. Stylianopoulos, and G. C. Alexandropoulos, "Evolving multi-branch attention convolutional neural networks for online RIS configuration," *IEEE TCCN*, 2025.

Centralized vs. Distributed RISs Optimization (1/2)

- When \mathcal{OP}_8 is solved **centrally** via a GPU (e.g., the BS), instantaneous CSI needs to be gathered. The optimized phase configurations of the RISs need to be shared to their controllers via dedicated control links.
- In this case, the input and the output matrices of the NN will exhibit a K -fold increase, and the mapping function might be too complicated to efficiently approximate and optimize.
- Even during inference time, the size of the NN may be too computationally demanding to support real-time control.

F. Saggese, V. Croisfelt, R. Kotaba, K. Stylianopoulos, G. C. Alexandropoulos, and P. Popovski,, "On the impact of control signaling in RIS-empowered wireless communications," *IEEE OJCOM*, 2024.

G. Stamatelis, K. Stylianopoulos, and G. C. Alexandropoulos, "Evolving multi-branch attention convolutional neural networks for online RIS configuration," *IEEE TCCN*, 2025.

Centralized vs. Distributed RISs Optimization (2/2)

- Consider a hybrid RIS capable of channel estimation which also incorporates a GPU in each controller to solve \mathcal{OP}_8 .
- With such a **distributed** setup, policy approximation could be easier, since each distinct processing unit would be equipped with a lighter NN.
- In particular, each distributed processing unit could use an identical copy of the optimized NN to learn the mapping function for a single RIS.

G. C. Alexandropoulos, N. Shlezinger, I. Alamzadeh, M. F. Imani, H. Zhang, and Y. C. Eldar, "Hybrid reconfigurable intelligent metasurfaces: Enabling simultaneous tunable reflections and sensing for 6G wireless communications," *IEEE VTM*, 2024.

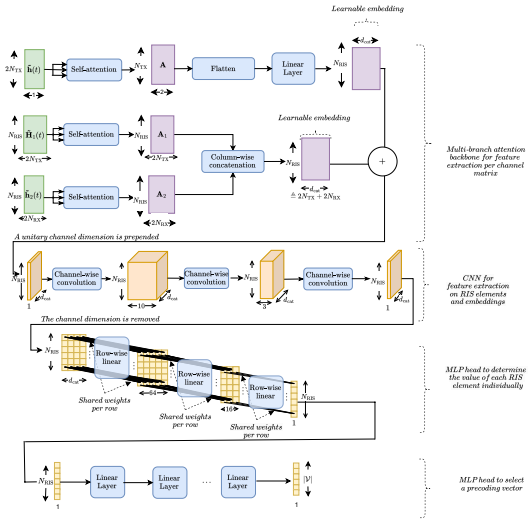
G. Stamatelis, K. Stylianopoulos, and G. C. Alexandropoulos, "Evolving multi-branch attention convolutional neural networks for online RIS configuration," *IEEE TCCN*, 2025.

The Proposed MBACNN Architecture

- First, attention modules extract sequential correlations in the channel matrices.
- Then, the extracted features are summed into one image-like matrix.
- Batch normalization is used to enhance stability.
- Convolution layers are used to decrease dimensions and extract geometric information.
- One element-wise DNN is responsible for the RIS phase profile selection.
- One more DNN module selects the TX precoding vector.

G. Stamatelis, K. Stylianopoulos, and G. C. Alexandropoulos, "Evolving multi-branch attention convolutional neural networks for online RIS configuration," *IEEE TCCN*, 2025.

The Proposed MBACNN Architecture (Schematically)



G. Stamatelis, K. Stylianopoulos, and G. C. Alexandropoulos, "Evolving multi-branch attention convolutional neural networks for online RIS configuration," *IEEE TCCN*, 2025.

Optimization via Neuroevolution

- Consider a system with only the k -th RIS. The fitness function for an individual NN over a sample of T_E episodes is computed as:

$$f \triangleq \frac{1}{T_E} \sum_{t_e=1}^{T_E} \frac{1}{T} \sum_{t=1}^T \gamma(g_w(\mathbf{h}(t), \mathbf{H}_{1,k}(t), \mathbf{h}_{2,k}(t))) .$$

- Each has horizon T .
- For each time instant $t \leq T$, sample the channels $\mathbf{h}(t)$, $\mathbf{H}_{1,k}(t)$, and $\mathbf{h}_{2,k}(t)$, which are then provided to the NN to output $\Phi_k(t)$ and $\mathbf{v}(t)$.
- The instantaneous SNR is calculated and stored.
- This optimization is performed with the Cooperative SYnamptic NEuroevolution (CoSyNe) algorithm.

F. Gomez *et al.*, "Accelerated neural evolution through cooperatively coevolved synapses," *JMLR*, 2008.

G. Stamatelis, K. Stylianopoulos, and G. C. Alexandropoulos, "Evolving multi-branch attention convolutional neural networks for online RIS configuration," *IEEE TCCN*, 2025.

Why Neuroevolution?

- It has been experimentally shown that even simple NE schemes can rival back-propagation algorithms, such as Q -learning and policy gradients, outperforming DRL approaches in various single-agent POMDPs.
- NE is easier to implement (replay buffers, advantage estimation, etc. are not needed) and to parallelize over multiple CPUs.
- Reward reshaping and exploration techniques are not required in NE schemes.
- DRL schemes face instability problems, which are associated with back-propagation through time; this issue is absent in NE.

F. Gomez *et al.*, "Accelerated neural evolution through cooperatively coevolved synapses," *JMLR*, 2008.

G. Stamatelis, K. Stylianopoulos, and G. C. Alexandropoulos, "Evolving multi-branch attention convolutional neural networks for online RIS configuration," *IEEE TCCN*, 2025.

How Does Neuroevolution Work?

- It directly searches the space of the policy NNs via nature-inspired algorithms, i.e., no critic NNs considered; each chromosome of an individual represents some parameters of a policy NN.
- Techniques that take advantage of the NN's structure to construct fewer individuals are usually devised.
- Initially, generate individuals randomly; compute and store each individual's fitness function; the individuals with the highest fitness functions are selected for mating. During mating, the parameters of two or more individuals are merged by various methods (e.g., crossover operation). The new individuals then replace the “weaker” ones of the population.

F. Gomez *et al.*, “Accelerated neural evolution through cooperatively coevolved synapses,” *JMLR*, 2008.

G. Stamatelis, K. Stylianopoulos, and G. C. Alexandropoulos, “Evolving multi-branch attention convolutional neural networks for online RIS configuration,” *IEEE TCCN*, 2025.

Distributed Optimization via Neuroevolution

- The proposed solution consists of a lightweight messaging protocol and a decentralized parameter sharing evolution approach based on CoSyNE.
- The designed MBACNN architecture is enriched with only an additional MLP module to distributedly decide each $\phi_k(t)$ (the previous four modules $g_w^{(1:4)}$ and the newly added $g_w^{(5)}(\cdot)$ module).
- \mathcal{OP}_8 is solved via $K + 1$ agents:
 - ① Each k -th of the first K agents decides each $\phi_k(t)$.
 - ② The final $(K + 1)$ -th agent, which is placed at the RX side, is responsible for deciding $v(t)$, and consequently, feeding it back to the TX. This agent receives lightweight messages from the K RIS agents, which are passed to a separate NN as side information so that $v(t)$ is decided.

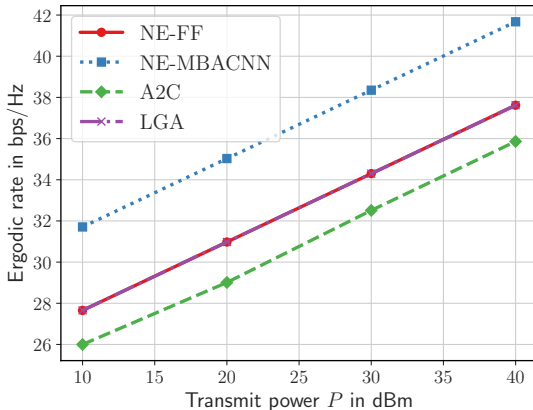
G. Stamatelis, K. Stylianopoulos, and G. C. Alexandropoulos, "Evolving multi-branch attention convolutional neural networks for online RIS configuration," *IEEE TCCN*, 2025.

Simulation Setup

- TX positioned at $(0, 0, 2.0)$ m, RIS placed in LOS with the TX at $(0, 3, 2.0)$ m, and RX at $(8, 10, 1.5)$ m.
- $N_{\text{TX}} = 16$, $N_{\text{RIS}} = 400$, and $K = 1$.
- Ricean channels with $\kappa = 10$ dB.
- TX power varied from 10 to 40 dBm; noise level set to -50 dBm.
- Benchmarks: Advantage Actor Critic (A2C); Lightweight Genetic Algorithm (LGA); and NE with Feed-Forward NNs (NE-FF).

G. Stamatelis, K. Stylianopoulos, and G. C. Alexandropoulos, "Evolving multi-branch attention convolutional neural networks for online RIS configuration," *IEEE TCCN*, 2025.

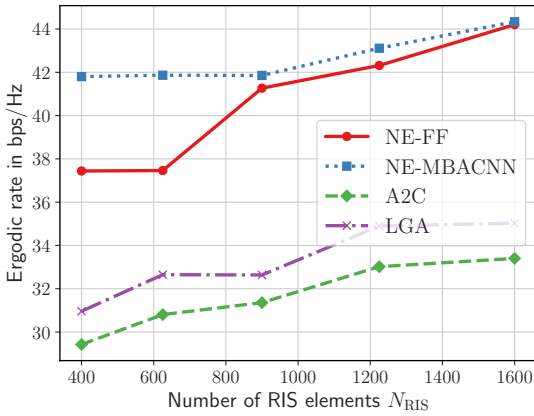
Ergodic Rate vs. TX Power



NE-MBACNN outperforms all baselines; interestingly, NE-FF outperforms A2C highlighting the NE potential.

G. Stamatelis, K. Stylianopoulos, and G. C. Alexandropoulos, "Evolving multi-branch attention convolutional neural networks for online RIS configuration," *IEEE TCCN*, 2025.

Ergodic Rate vs. RIS size



NE's superiority is maintained for large RIS sizes.

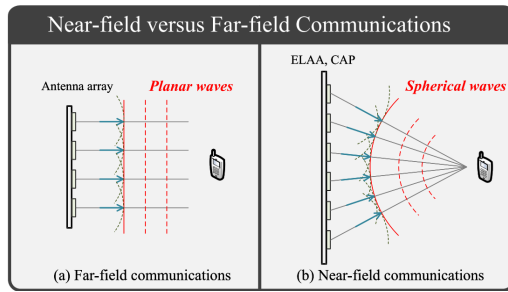
G. Stamatelis, K. Stylianopoulos, and G. C. Alexandropoulos, "Evolving multi-branch attention convolutional neural networks for online RIS configuration," *IEEE TCCN*, 2025.

1 Part III: Distributed Sensing-Aided Communications

- Optimization of Multi-RIS-Aided Communications
- Distributed Learning for Multi-RIS-Aided Communications
- Position-Aided Near-Field Beam Tracking
- Sensing-Aided Communications via Hydrid RISs
- Over-the-Air Learning: The XL MIMO Potential

Near-Field Communications

- The interplay between large antenna apertures and high frequencies in future generations of wireless networks will give rise to near-field communications.
- This form of communications brings forth a paradigm shift compared to angular-based BF techniques and channel modeling, since the curvature of the spherical wavefront becomes non-negligible.



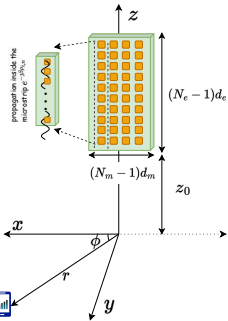
Y. Liu, Z. Wang, J. Xu, C. Ouyang, X. Mu and R. Schober, "Near-field communications: A tutorial review," *IEEE OJCOM*, 2023.

The Near-Field Beam Tracking Problem

- This near-field transition raises several open questions:
 - What is the distance limit up to which far-field approximation is effective for path gain prediction and beam design?
 - What is the resolution with which the position of the BF target should be known for accurate BF in the near-field regime (a.k.a. beam focusing)?
 - How frequently CSI knowledge is needed in order to follow a moving target with highly directive beams without losing QoS-based focus?
- An analysis of the BF gain degradation, due to outdated focusing, is next presented together with the novel metric of *beam coherence time*.

P. Gavriilidis and G. C. Alexandropoulos, "Near-field beam tracking with extremely massive dynamic metasurface antennas," *IEEE TWC*, 2025.

System Model (1/2)



- A DMA-based XL MIMO BS with single-RF-fed microstrips at $f_c > 30$ GHz wishes to communicate with a single-antenna UE: BF towards the UE location to achieve the maximum possible gain therein.

N. Shlezinger *et al.*, "Dynamic metasurface antennas for 6G extreme massive MIMO communications," *IEEE WCOM*, 2021.

P. Gavriilidis and G. C. Alexandropoulos, "Near-field beam tracking with extremely massive dynamic metasurface antennas," *IEEE TWC*, 2025.

System Model (2/2)

- The beam depth/width are limited according to the DMA's physical dimensions and the UE's location relative to the former.
- Changes in UE's coordinates from the focusing position might not affect the achievable beamforming gain.
- The resolution of the UE's coordinates to be estimated could be sparser as the UE moves further away from the BS, while keeping the BF gain to the maximum.
- Adopting both reconfigurable time intervals between estimations as well as reconfigurable localization resolution relative to the UE's current location.

P. Gavriilidis and G. C. Alexandropoulos, "Near-field beam tracking with extremely massive dynamic metasurface antennas," *IEEE TWC*, 2025.

BF Gain under Coordinate Mismatch (1/4)

- **Goal:** Quantify the BF gain degradation due to mismatch between focusing position and the actual UE position (r, ϕ) in the near-field regime.
- The relative beamforming gain under coordinate mismatch is given as: $\frac{G_{\hat{r}, \hat{\phi}}}{G_{\text{opt}}}$, with $G_{\hat{r}, \hat{\phi}} \triangleq |\mathbf{a}^H(\hat{r}, \hat{\phi})\mathbf{a}(r, \phi)|^2$.
- $G_{\text{opt}} = N^2$ (square of BS's elements) and $\mathbf{a}(r, \phi)$ is the beam focusing vector.
- **Analytical model:** The normalized BF gain loss has been approximated as:

$$\frac{G_{\hat{r}, \hat{\phi}}}{G_{\text{opt}}} \approx \mathcal{M}(\hat{r}, \hat{\phi}) = I(\hat{r})\mathcal{L}(\hat{\phi})$$

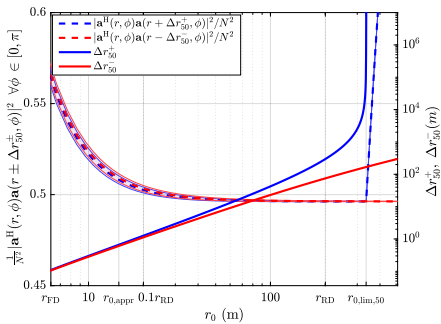
where $I(\cdot)$ and $\mathcal{L}(\cdot)$ quantify losses due to radial and angular mismatches.

P. Gavriilidis and G. C. Alexandropoulos, "Near-field beam tracking with extremely massive dynamic metasurface antennas," *IEEE TWC*, 2025.

BF Gain under Coordinate Mismatch (2/4)

- The latter decoupled model enables closed-form prediction of the beamdepth and beamwidth.
- Radial region: $\frac{G_{\hat{r}, \phi}}{G_{\text{opt}}} \geq \kappa\%$ for $\hat{r} \in [r - \Delta r_{\kappa}^-, r + \Delta r_{\kappa}^+]$.
 - $\Delta r_{\kappa}^{\pm} = r^2 \left(\frac{2d_e^2(N_e-1)^2}{\lambda a_{\kappa}^2} \mp r \right)^{-1}$, where a_{κ} is an auxiliary variable that depends on the threshold κ .
 - These limits are asymmetrical: Δr_{κ}^- indicates a direction of movement towards the BS, while Δr_{κ}^+ away from it.
- Angular region: $\frac{G_{r, \hat{\phi}}}{G_{\text{opt}}} \geq \kappa\%$ for $\hat{\phi} \in [\phi - \Delta \phi_{\kappa}, \phi + \Delta \phi_{\kappa}]$.
 - $\Delta \phi_{\kappa} = \left| \frac{\zeta_{\kappa} \lambda}{\pi N_m d_m \sin(\phi)} \right|$, where ζ_{κ} is an auxiliary variable that depends on the threshold κ .

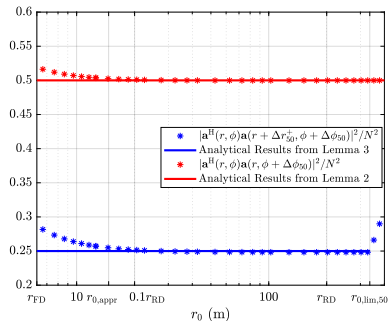
BF Gain under Coordinate Mismatch (3/4)



- We have numerically evaluated $\frac{|G(\hat{r}, \phi)|^2}{N^2} \forall \phi \in [0, \pi]$ for $\kappa\% = 50\%$.
- Δr_{50}^+ has a steeper rate of change compared to Δr_{50}^- , indicating that the radial regions become increasingly asymmetrical as r_0 increases.
- Key Insight:** Δr_κ^- depicts the direction of UE movement towards the BS, where the near-field effects are stronger, hence, $\Delta r_\kappa^- \leq \Delta r_\kappa^+$.

P. Gavriilidis and G. C. Alexandropoulos, "Near-field beam tracking with extremely massive dynamic metasurface antennas," *IEEE TWC*, 2025.

BF Gain under Coordinate Mismatch (4/4)



- Sufficiently tight analytical results for $r_0 \geq r_{0,appr}$; interestingly, the approximations are satisfactory even before this distance value.
- This is the first work that provides a decoupled analytical function in both the range r and the azimuth angle ϕ for the beam focusing gain achieved with a planar-array-type TX.

P. Gavriilidis and G. C. Alexandropoulos, "Near-field beam tracking with extremely massive dynamic metasurface antennas," *IEEE TWC*, 2025.

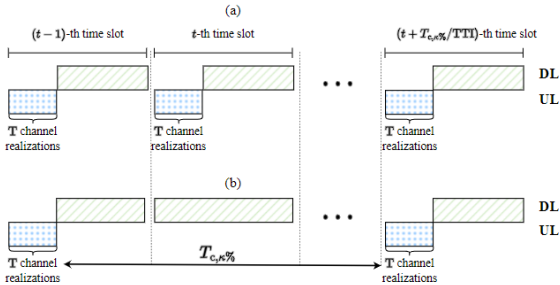
Direction of Fastest BF Gain Deterioration

- Assume a UE movement of c meters in the xy -plane from its last position (r, ϕ) ; following the cosine law, the new position will be $\left(r + d, \phi \pm \arccos\left(1 - \frac{c^2 - d^2}{2r^2 + 2rd}\right)\right)$ with $|d| \leq c$.
- The relative BF function $\mathcal{M}(\cdot, \cdot)$ can be re-expressed for a given c as $\mathcal{M}(d) = I(r + d)\mathcal{L}\left(\phi \pm \arccos\left(1 - \frac{c^2 - d^2}{2r^2 + 2rd}\right)\right)$; solving $d_{\min} \triangleq \min_d \mathcal{M}(d)$ yields the direction of the fastest BF descent.
- Hence, the minimum distance needed, $c_{\min, \kappa\%}$, so that the beamforming gain drops to $\kappa\%$ of its optimum value G_{opt} can be obtained.
- Let u be the norm of the UE's velocity, we define the **beam coherence time** that indicates the minimum time needed for the BF gain to drop to $\kappa\%$ of G_{opt} as:

$$T_{c, \kappa\%} \triangleq \frac{c_{\min, \kappa\%}}{u}.$$

P. Gavriilidis and G. C. Alexandropoulos, "Near-field beam tracking with extremely massive dynamic metasurface antennas," *IEEE TWC*, 2025.

Proposed QoS-Aware Protocol Beam Tracking



- The BS requests pilot signals at $T_{c,\kappa\%}$ intervals for UE position estimation, thus maintaining the BF gain above $\kappa\%$.
- This ensures stable and reliable communication without frequent estimations, adapting to near-field phenomena and to different QoS by means of tuning $\kappa\%$.

P. Gavriilidis and G. C. Alexandropoulos, "Near-field beam tracking with extremely massive dynamic metasurface antennas," *IEEE TWC*, 2025.

Dynamic Non-Uniform Grid Design (1/2)

- The localization objective is expressed as a BF gain objective, i.e.:

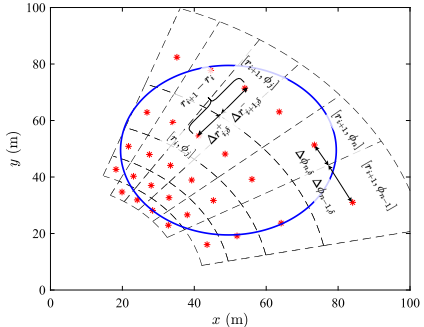
$$\text{find } (\hat{r}, \hat{\phi}) \text{ so that } G_{\hat{r}, \hat{\phi}} \approx G_{\text{opt}}.$$

- The sampling resolution of r and ϕ will be given relative to how close we wish to reach the optimum BF gain.
- To achieve $\delta\%$ of G_{opt} , each sampling point (r_i, ϕ_j) is chosen to have a decision area such that, $\forall \hat{r}$ and $\forall \hat{\phi}$ within this area, it holds that:

$$\frac{G_{\hat{r}, \phi_j}}{G_{\text{opt}}}, \frac{G_{r_i, \hat{\phi}}}{G_{\text{opt}}} \geq \delta\%.$$

- The ensemble of the sampling points is selected so that their decision areas cover the whole of the area of interest with the minimum number of samples.

Dynamic Non-Uniform Grid Design (2/2)



The sampled grid for a circular area of interest with central point at the polar coordinates $r = 70$ m and $\phi = \pi/4$ rad, resolution $\delta\% = 80\%$, and radius $c = 30$ m.

- When $\phi_i \rightarrow 0$, yields $\sin(\phi_i) \rightarrow 0$, thus, angular distances become wider following the derived angular limits.
- For the radial limits, Δr_i^\pm increases with increasing r .

P. Gavriilidis and G. C. Alexandropoulos, "Near-field beam tracking with extremely massive dynamic metasurface antennas," *IEEE TWC*, 2025.

Proposed Near-Field Beam Tracking Algorithm

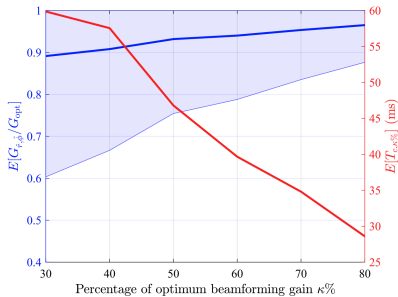
Algorithm 2 Proposed Near-Field Beam Tracking

Input: Localization resolution $\delta\%$, percentage of optimum beamforming gain $\kappa\%$, previous estimates $\hat{u}_0, \dots, \hat{u}_{t-1}, \hat{p}_{t-1}$, and $T_{c,\kappa\%}(t-1)$, e_c and e_u , and total number of pilots N_p .

- 1: The time interval $T_{c,\kappa\%}(t-1)$ from the previous $(t-1)$ -th estimation slot elapsed, request UE pilots' transmission.
 - 2: Set the radius of the UE area of interest as $\hat{c} = c_{\kappa\%}(1+e_c)$.
 - 3: Run Alg. 1 using \hat{r}_{t-1} , $\hat{\phi}_{t-1}$, \hat{c} , and $\delta\%$, to obtain $(r_{s_r}, [\phi_{s_r}]_i) \forall s_r = 1, 2, \dots, S_r$, and $\forall i = 1, 2, \dots, S_{\phi_{s_r}}$.
 - 4: Perform the initializations $\mathbf{g} = \mathbf{0}_{S_r \times 1}$ and $\mathbf{K} = \mathbf{0}_{S_r \times 2}$.
 - 5: Set the averaging per Q configuration to $M = \lfloor N_p / S_r \rfloor$.
 - 6: **for** $s_r = 1, 2, \dots, S_r$ **do**
 - 7: Obtain $\bar{\mathbf{Q}}_{s_r}$ via (13) to steer on range r_{s_r} .
 - 8: Collect the measurements $\mathbf{y}_{b,r_{s_r}}[1], \dots, \mathbf{y}_{b,r_{s_r}}[M]$ as in (8) for different noise realizations.
 - 9: Compute the average $\bar{\mathbf{y}}_{b,r_{s_r}} = M^{-1} \sum_{m=1}^M \mathbf{y}_{b,r_{s_r}}[m]$.
 - 10: Calculate $i_{\max} = \arg \max_i |\mathbf{v}_{[\phi_{s_r}]_i}^H \bar{\mathbf{y}}_{b,r_{s_r}}|^2$ and set $[\mathbf{g}]_{s_r} = |\mathbf{v}_{[\phi_{s_r}]_{i_{\max}}}^H \bar{\mathbf{y}}_{b,r_{s_r}}|^2$ and $[\mathbf{K}]_{s_r,:} = [r_{s_r}, [\phi_{s_r}]_{i_{\max}}]$.
 - 11: **end for**
 - 12: Set $s_{r_{\max}} = \arg \max_i [\mathbf{g}]_i$ and $\hat{\mathbf{p}}_t = [\hat{r}_t, \hat{\phi}_t] = [\mathbf{K}]_{s_{r_{\max}},:}$.
 - 13: Update the velocity estimate as $\hat{u}_t = \frac{||\hat{\mathbf{p}}_t - \hat{\mathbf{p}}_{t-1}||_2}{T_{c,\kappa\%}(t-1)}$.
 - 14: Compute the velocity estimate \hat{u}_{t+1} using (15) and the previous estimates $(\hat{u}_0, \hat{u}_1, \dots, \hat{u}_t)$.
 - 15: $c_{\kappa\%} = \min \left\{ |2\hat{r}_t \sin(0.5\Delta_{\kappa}(\hat{\phi}_t))|, \Delta_{\kappa}(\hat{r}_t) \right\}$ via (9), (11).
 - 16: Compute the effective beam coherence time for triggering the $(t+1)$ -th estimation slot as $T_{c,\kappa\%}(t) = \frac{c_{\kappa\%}}{\hat{u}_{t+1}(1+e_u)}$.
- Output:** $\hat{\mathbf{p}}_t$, \hat{u}_t , and $T_{c,\kappa\%}(t)$.
-

P. Gavriilidis and G. C. Alexandropoulos, "Near-field beam tracking with extremely massive dynamic metasurface antennas," *IEEE TWC*, 2025.

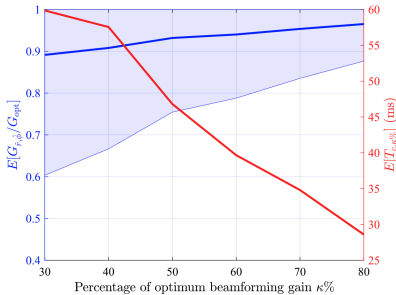
BF Gain and Estimation Time vs κ (1/2)



- Left y-axis: Average relative beamforming gain $E \left[G_{\hat{r},\hat{\phi}} / G_{\text{opt}} \right]$ and 95th percentile errorbar over time with $500 \mu\text{s}$ time step.
- Right y-axis: Average estimation time interval $E [T_{c,\kappa\%}]$.
- The x-axis represents different QoS constraints modeled via κ ; higher values lead to stricter constraints.

P. Gavriilidis and G. C. Alexandropoulos, "Near-field beam tracking with extremely massive dynamic metasurface antennas," *IEEE TWC*, 2025.

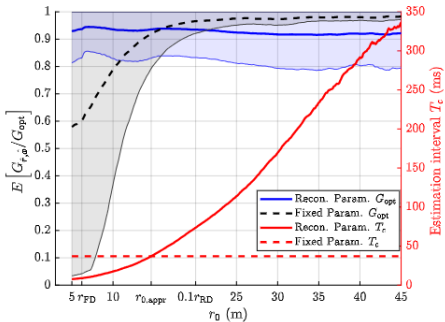
BF Gain and Estimation Time vs κ (2/2)



- By employing the reconfigurable estimation interval $T_{c,\kappa%}$, the percentage of gain achieved is always greater than $\kappa\%$.
- As anticipated, $T_{c,\kappa%}$ decreases with increasing $\kappa\%$, since denser estimations are needed over time to satisfy a stricter $\kappa\%$ constraint.

P. Gavriilidis and G. C. Alexandropoulos, "Near-field beam tracking with extremely massive dynamic metasurface antennas," *IEEE TWC*, 2025.

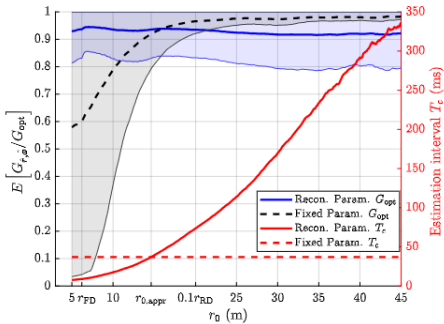
BF Gain and Estimation Time vs r_0 (1/2)



- The x-axis represents the distance of the user from the BS's center r_0 .
- The blue and black lines correspond to the proposed framework and the fixed parameter benchmark, respectively, i.e., fixed T and localization resolution $\Delta r_{\text{fix}}, \Delta\phi_{\text{fix}}$ set as the averages of the former for $\kappa\% = 50\%$.

P. Gavriilidis and G. C. Alexandropoulos, "Near-field beam tracking with extremely massive dynamic metasurface antennas," *IEEE TWC*, 2025.

BF Gain and Estimation Time vs r_0 (2/2)



- Although the estimation intervals increase with increasing r_0 , the BF gain achieved remains stable always exceeding $\kappa\% = 50\%$.
- For the fixed parameter scenario, although the average BF gain is stabilized after $r_0 \geq 0.1r_{RD}$, it is extremely unreliable for shorter distances.
- Both scenarios have the same average estimation interval, the proposed does a smart allocation by dense estimations at small r_0 and sparser as r_0 increases.

P. Gavriilidis and G. C. Alexandropoulos, "Near-field beam tracking with extremely massive dynamic metasurface antennas," *IEEE TWC*, 2025.

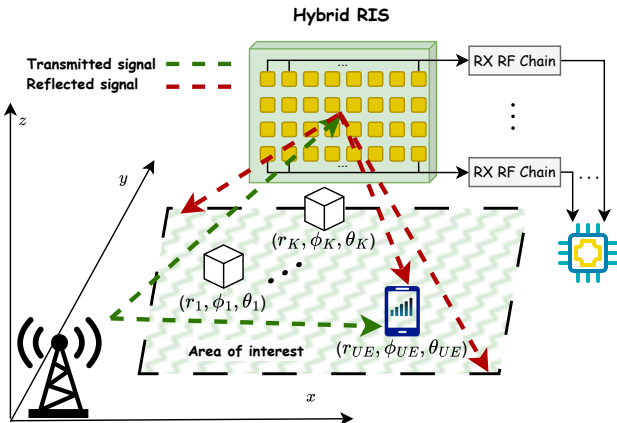
Future Directions

- Multi-user near-field beam tracking: extending the analysis for the beam coherence time and beam depth/width metrics under multiple focusing beams from the BS.
- Trajectory-aware tracking via probabilistic path modeling (e.g., fitting with motion priors).
- Multi-BS coordination for joint near-field beam tracking and coverage optimization.

1 Part III: Distributed Sensing-Aided Communications

- Optimization of Multi-RIS-Aided Communications
- Distributed Learning for Multi-RIS-Aided Communications
- Position-Aided Near-Field Beam Tracking
- Sensing-Aided Communications via Hydrid RISs
- Over-the-Air Learning: The XL MIMO Potential

The Proposed HRIS-Enabled ISAC System



I. Gavras and G. C. Alexandropoulos, "Simultaneous communications and sensing with hybrid reconfigurable intelligent surfaces," *Proc. EuCAP*, 2025.

HRIS Operation Modeling

- M identical power splitters divide the power of the impinging signal at each hybrid meta-atom in the respective parts. For the sensing operation, to feed the absorbed portion of the impinging signal to the M_{RF} RX RF chains, the HRIS applies the analog combining matrix $\mathbf{W} \in \mathbb{C}^{M \times M_{\text{RF}}}$:

$$[\mathbf{W}]_{(l-1)M_E+m,j} = \begin{cases} w_{l,m}, & l = j \\ 0, & l \neq j \end{cases},$$

where $|w_{l,m}| = 1$ (with $m = 1, 2, \dots, M$ and $l = 1, 2, \dots, M_{\text{RF}}$).

- The HRIS reflection configuration is represented by $\phi \in \mathbb{C}^{M \times 1}$ with $|[\phi]_m| = 1 \forall m$.
- The BS precodes digitally via the channel-dependent BF vector $\mathbf{v} \in \mathbb{C}^{N \times 1}$ each complex-valued symbol s such that $\mathbb{E}\{\|\mathbf{v}s\|^2\} \leq P_{\max}$, where P_{\max} is the maximum transmission power.

I. Gavras and G. C. Alexandropoulos, "Simultaneous communications and sensing with hybrid reconfigurable intelligent surfaces," *Proc. EuCAP*, 2025.

Near-Field Channel Model (1/2)

- The sub-THz $M \times N$ complex-valued channel matrix between the BS and the HRIS is modeled as:

$$[\mathbf{H}_{\text{BR}}]_{(I-1)M_{\text{E}}+m,n} \triangleq \alpha_{I,m,n} \exp\left(\frac{j2\pi}{\lambda} r_{I,m,n}\right)$$

with $r_{I,m,n}$ denoting the distance between each m -th element of each I -th RX RF chain at the HRIS and the n -th (with $n = 1, 2, \dots, N$) BS antenna.

- Let the spherical coordinates of the K potentially present passive radar targets within the area of interest denoted by $\{(r_k, \theta_k, \varphi_k)\}$,
 $\forall k = 1, 2, \dots, K$; the end-to-end channel matrix:

$$\begin{aligned} \mathbf{H}_{\text{R}} &\triangleq \sum_{k=1}^K \beta_k \mathbf{a}_{\text{RX}}(r_k, \theta_k, \varphi_k) \mathbf{a}_{\text{TX}}^{\text{H}}(r_k, \theta_k, \varphi_k) \\ &+ \beta_{\text{UE}} \mathbf{a}_{\text{RX}}(r_{\text{UE}}, \theta_{\text{UE}}, \varphi_{\text{UE}}) \mathbf{a}_{\text{TX}}^{\text{H}}(r_{\text{UE}}, \theta_{\text{UE}}, \varphi_{\text{UE}}). \end{aligned}$$

I. Gavras and G. C. Alexandropoulos, "Simultaneous communications and sensing with hybrid reconfigurable intelligent surfaces," *Proc. EuCAP*, 2025.

Near-Field Channel Model (2/2)

- β_k and β_{UE} represent the complex-valued reflection coefficients for each k -th (with $k = 1, 2, \dots, K$) radar target and the UE, respectively, and $\forall l, m, n$:

$$[\mathbf{a}_{\text{TX}}(r, \theta, \varphi)]_n \triangleq a_n \exp\left(j \frac{2\pi}{\lambda} r_n\right),$$

$$[\mathbf{a}_{\text{RX}}(r, \theta, \varphi)]_{(l-1)M_{\text{E}}+m} \triangleq a_{l,m} \exp\left(j \frac{2\pi}{\lambda} r_{l,m}\right),$$

- The channel between the BS and the UE is represented as $\mathbf{h}_{\text{BU}} \triangleq \mathbf{a}_{\text{TX}}(r_{\text{UE}}, \theta_{\text{UE}}, \varphi_{\text{UE}})$, while the channel between the UE and the HRIS as $\mathbf{h}_{\text{RU}} \triangleq \mathbf{a}_{\text{RX}}^T(r_{\text{UE}}, \theta_{\text{UE}}, \varphi_{\text{UE}})$ with $(r_{\text{UE}}, \theta_{\text{UE}}, \varphi_{\text{UE}})$ denoting the spherical coordinates of the UE.

I. Gavras and G. C. Alexandropoulos, "Simultaneous communications and sensing with hybrid reconfigurable intelligent surfaces," *Proc. EuCAP*, 2025.

Received Signals

- The baseband received signal at the UE can be mathematically expressed as:

$$y \triangleq (\mathbf{h}_{\text{BU}} + (1 - \rho)\mathbf{h}_{\text{RU}}\text{diag}(\phi)\mathbf{H}_{\text{BR}})\mathbf{v}\mathbf{s} + n,$$

where $(1 - \rho)$ represents the absorption portion of the impinging signal at every hybrid meta-atom, with $\rho \in [0, 1]$ being the common power splitting ratio.

- Assuming T BS transmissions per coherent channel block and that the static BS-HRIS channel can be completely cancelled, the baseband received signal $\mathbf{Y} \in \mathbb{C}^{M_{\text{RF}} \times T}$ at the outputs of the M_{RF} RX RF chains of the HRIS is modeled as:

$$\mathbf{Y} = [\mathbf{y}(1), \mathbf{y}(2), \dots, \mathbf{y}(T)] \triangleq \rho \mathbf{W}^H \mathbf{H}_R \mathbf{v} \mathbf{s} + \mathbf{N}.$$

I. Gavras and G. C. Alexandropoulos, "Simultaneous communications and sensing with hybrid reconfigurable intelligent surfaces," *Proc. EuCAP*, 2025.

PEB Analysis

- $\mathbf{y} \sim \mathcal{CN}(\mathbf{M}, \mathbf{R}_n)$ with $\mathbf{M} \triangleq \rho \mathbf{W}^H \mathbf{H}_R \mathbf{v} \mathbf{s}$ and $\mathbf{R}_n \triangleq \sigma^2 \mathbf{I}_{M_{RF}}$. To estimate each k -th passive radar parameters $\zeta \triangleq [r, \theta, \varphi]^T$, each (i, j) -th element the 3×3 FIM, \mathbf{I} , is computed as:

$$[\mathbf{I}]_{i,j} \triangleq 2\text{Re} \left\{ \frac{\partial \mathbf{M}^H}{\partial [\zeta]_i} \mathbf{R}_n^{-1} \frac{\partial \mathbf{M}}{\partial [\zeta]_j} \right\} + \text{Tr} \left\{ \mathbf{R}_n^{-1} \frac{\partial \mathbf{R}_n}{\partial [\zeta]_i} \mathbf{R}_n^{-1} \frac{\partial \mathbf{R}_n}{\partial [\zeta]_j} \right\}.$$

- Each diagonal element of the FIM is calculated as:

$$[\mathbf{I}]_{i,i} = \frac{2\rho^2}{\sigma^2} \text{Re} \left\{ \mathbf{s}^H \mathbf{v}^H \frac{\partial \mathbf{H}_R^H}{\partial [\zeta]_i} \mathbf{W} \mathbf{W}^H \frac{\partial \mathbf{H}_R}{\partial [\zeta]_i} \mathbf{v} \mathbf{s} \right\}.$$

- The PEB for each k -th target with true, but unknown, position ζ is expressed as $\text{PEB}_\zeta \triangleq \sqrt{\text{CRB}_\zeta} = \sqrt{\text{Tr} \{ \mathbf{I}^{-1} \}}$.

I. Gavras and G. C. Alexandropoulos, "Simultaneous communications and sensing with hybrid reconfigurable intelligent surfaces," *Proc. EuCAP*, 2025.

Problem Formulation

- After estimating the DL channel as $\hat{\mathbf{h}}_{\text{DL}} \triangleq \hat{\mathbf{h}}_{\text{BU}} + (1 - \rho)\hat{\mathbf{h}}_{\text{RU}}\text{diag}(\boldsymbol{\gamma})\hat{\mathbf{H}}_{\text{BR}}$, formulate the ISAC mathematical problem:

$$\begin{aligned}\mathcal{OP}_9 : \max_{\mathbf{W}, \phi, \mathbf{v}} \quad & \log_2 \left(1 + \sigma^{-2} \|\hat{\mathbf{h}}_{\text{DL}} \mathbf{v}\|^2 \right) \\ \text{s.t. } \text{PEB}_q \leq \gamma_s \quad & \forall q, |[\mathbf{w}]_{l,m}| = 1 \quad \forall l, m, \|\mathbf{v}\|^2 \leq P_{\max}.\end{aligned}$$

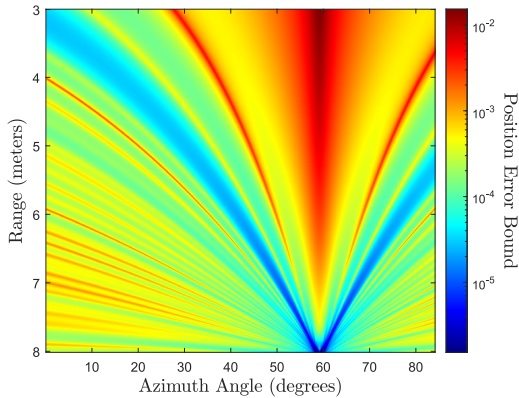
I. Gavras and G. C. Alexandropoulos, "Simultaneous communications and sensing with hybrid reconfigurable intelligent surfaces," *Proc. EuCAP*, 2025.

Simulation Parameters

- Bandwidth $B = 150$ kHz centered at the frequency of 120 GHz, where coherent channel blocks span $T = 200$ transmissions.
- Area of interest: $\theta = 30^\circ$, $\varphi \in [20^\circ, 80^\circ]$, and $r \in [0.62\sqrt{D^3/\lambda}, 2D^2/\lambda]$ meters with D being the HRIS diagonal length.
- Both the UE and the $K = 2$ radar targets were randomly positioned within the latter area, while the HRIS was considered placed at the point with $\theta_{\text{RIS}} = 30^\circ$, $\varphi_{\text{RIS}} = 60^\circ$, and $r_{\text{RIS}} = 8$ meters.
- The BS was equipped with a 2×8 UPA and the HRIS with $M_{\text{RF}} = 4$ RX RF chains each connected to $M_{\text{E}} = 64$ hybrid meta-atoms. AWGN's variance was set as $\sigma^2 = -174 + 10 \log_{10}(B)$.
- To evaluate localization coverage, we calculated the coverage capability as the percentage of 1000 equidistant discrete points within the area of interest.

I. Gavras and G. C. Alexandropoulos, "Simultaneous communications and sensing with hybrid reconfigurable intelligent surfaces," *Proc. EuCAP*, 2025.

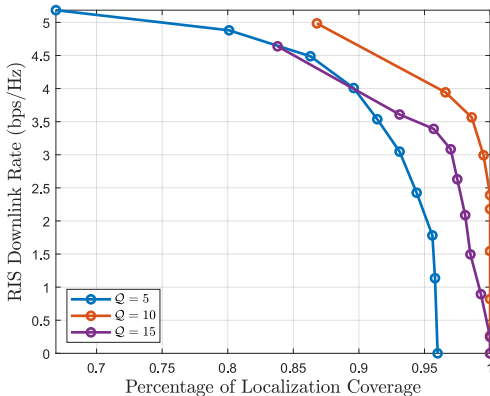
Area-Wide PEB



Setting: $P_{\max} = 16 \text{ dBm}$, $\gamma_s = 10^{-3}$, $\rho = 0.2$, and $Q = 5$.
The PEB threshold is met approximately at 80% of the desired area.

I. Gavras and G. C. Alexandropoulos, "Simultaneous communications and sensing with hybrid reconfigurable intelligent surfaces," *Proc. EuCAP*, 2025.

Achievable DL Rate vs. Localization Coverage

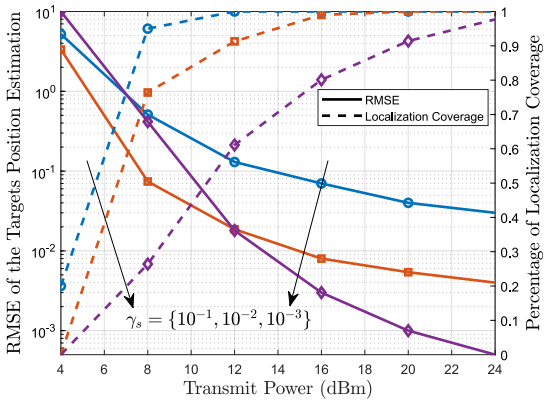


Setting: $P_{\max} = 16$ dBm and $\gamma_s = 10^{-3}$.

Increasing ρ improves localization coverage, while the communication performance get degraded.

I. Gavras and G. C. Alexandropoulos, "Simultaneous communications and sensing with hybrid reconfigurable intelligent surfaces," *Proc. EuCAP*, 2025.

Target Estimation and Localization Coverage



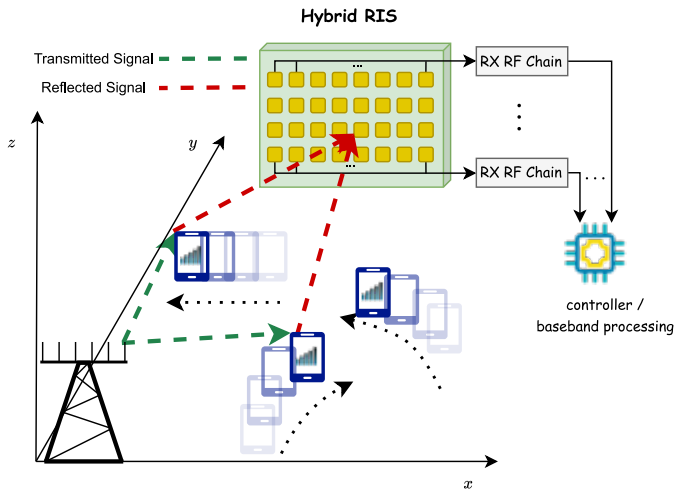
Setting: $\rho = 0.2$ and $Q = 5$.

Both metrics improve as SNR increase;

For increased localization coverage, the estimation performance per position gets degraded,
resulting also in decreased achievable DL rate.

I. Gavras and G. C. Alexandropoulos, "Simultaneous communications and sensing with hybrid reconfigurable intelligent surfaces," *Proc. EuCAP*, 2025.

Tracking-Aided Multi-User Communications



I. Gavras and G. C. Alexandropoulos, "Tracking-aided multi-user MIMO communications with hybrid reconfigurable intelligent surfaces," *arXiv preprint arXiv:2504.18846*, 2025.

System Model (1/2)

- The BS is equipped with an N_T -element ULA realizing fully digital TX BF, whereas the HRIS is modeled as a UPA with $N_H \triangleq N_{RF}N_E$ hybrid meta-atoms, where each column of elements is connected to a distinct RX RF chain (N_{RF} in total, with $N_H/N_{RF} \in \mathbb{Z}_*^+$), enabling partial signal absorption for baseband processing.
- The sensing capability of the HRIS is leveraged to track the UE trajectories.
- For the sensing operation, to feed the absorbed portion of the impinging signal to the N_{RF} RX RF chains, the HRIS applies the analog combining matrix $\mathbf{W}_H \in \mathbb{C}^{N_H \times N_{RF}}$, which is modeled as: $[\mathbf{W}_H]_{(I-1)N_E+n,j} = w_{I,n}$ for $I = j$ ($I, j = 1, \dots, N_{RF}$) and $[\mathbf{W}_H]_{(I-1)N_E+n,j} = 0$ for $I \neq j$, where $|w_{I,n}| = 1$ ($n = 1, \dots, N_H$) for each non-zero element in \mathbf{W}_H .
- The effective HRIS reflection coefficients are represented by $\varphi \in \mathbb{C}^{N_H \times 1}$ (i.e., the $1 - \varrho$ portion of the impinging signal), assuming that $|\varphi_n| = 1 \forall n$.

I. Gavras and G. C. Alexandropoulos, "Tracking-aided multi-user MIMO communications with hybrid reconfigurable intelligent surfaces," *arXiv preprint arXiv:2504.18846*, 2025.

System Model (2/2)

- OFDM is used for wideband DL communication, where the BS transmits T OFDM symbols over K subcarriers to U users in a per frame basis.
- To enable BF design for multi-UE tracking, $U \leq N_T \leq N_H$ is assumed. The transmit symbol matrix per frame is $\mathbf{S} \triangleq [\mathbf{S}_1, \dots, \mathbf{S}_K] \in \mathbb{C}^{KU \times T}$, with each $\mathbf{S}_k = [\mathbf{s}_{k,0}, \dots, \mathbf{s}_{k,U}] \in \mathbb{C}^{U \times T}$ and $\mathbf{s}_{k,u} \in \mathbb{C}^{T \times 1}$ denoting the data vector for UE u on subcarrier k .
- The joint precoding matrix is $\mathbf{F}_{\text{TX}} \triangleq \text{blkdiag}(\mathbf{F}_1, \dots, \mathbf{F}_K) \in \mathbb{C}^{KN_T \times KU}$, where each $\mathbf{F}_k = [\mathbf{f}_{k,0}, \dots, \mathbf{f}_{k,U}] \in \mathbb{C}^{N_T \times U}$, with $\mathbf{f}_{k,u} \in \mathbb{C}^{N_T \times 1}$, is the precoding vector for UE u . The transmit power satisfies $\mathbb{E}\{\|\mathbf{F}_{\text{TX}}\mathbf{S}\|^2\} \leq P_{\max}$.

I. Gavras and G. C. Alexandropoulos, "Tracking-aided multi-user MIMO communications with hybrid reconfigurable intelligent surfaces," *arXiv preprint arXiv:2504.18846*, 2025.

Received Signal Models

- Received signal at the u -th UE on the k -th subcarrier over T OFDM symbols:

$$y_{k,u} \triangleq (\mathbf{h}_{\text{DL},k,u} + (1 - \varrho) \mathbf{h}_{\text{HU},k,u} \text{diag}(\boldsymbol{\varphi}) \mathbf{H}_{\text{BR},k}) \mathbf{f}_{k,u} \mathbf{s}_{k,u} + n,$$

where $\mathbf{h}_{\text{HU},k,u} \in \mathbb{C}^{1 \times N_{\text{H}}}$ is channel vector between the HRIS and each u -th UE, $\mathbf{h}_{\text{DL},k,u} \in \mathbb{C}^{1 \times N_{\text{T}}}$ is the DL channel vector between the BS and each u -th UE, $\mathbf{H}_{\text{BR},k} \in \mathbb{C}^{N_{\text{H}} \times N_{\text{T}}}$ is the LoS BS-HRIS channel matrix, and $n \sim \mathcal{CN}(0, \sigma^2)$ is the AWGN vector.

- Given the end-to-end composite channel matrix $\mathbf{H}_H \in \mathbb{C}^{N_{\text{H}} \times N_{\text{T}}}$ between the HRIS and the BS, the baseband received signal at the N_{RF} RX RF chains of the HRIS for the k -th subcarrier is:

$$\mathbf{Y}_k = [\mathbf{y}_k(1), \dots, \mathbf{y}_k(T)] \triangleq \varrho \mathbf{W}_H^H \mathbf{H}_{H,k} \mathbf{F}_k \mathbf{S}_k + \mathbf{N},$$

where $\mathbf{N} \triangleq [\mathbf{n}(1), \dots, \mathbf{n}(T)] \in \mathbb{C}^{N_{\text{RF}} \times T}$, with $\mathbf{n}(t) \sim \mathcal{CN}(0, \sigma^2 \mathbf{I}_{N_{\text{RF}}}) \forall t$, is the matrix with the AWGN vectors per received OFDM symbol.

I. Gavras and G. C. Alexandropoulos, "Tracking-aided multi-user MIMO communications with hybrid reconfigurable intelligent surfaces," *arXiv preprint arXiv:2504.18846*, 2025.

PEB Analysis (1/2)

- Let $\boldsymbol{\eta} \in \mathbb{R}^{6U \times 1}$ and $\tilde{\boldsymbol{\eta}} \in \mathbb{R}^{4U \times 1}$ be respectively the channel- and location-domain parameter vectors within a frame. It holds that $\mathbf{y}_k \triangleq \text{vec}\{\mathbf{Y}_k\} \sim \mathcal{CN}(\boldsymbol{\mu}_k, \sigma^2 \mathbf{I}_{N_{\text{RF}} T})$ with mean $\boldsymbol{\mu}_k \triangleq \text{vec}\{\varrho \mathbf{W}_H^H \mathbf{H}_{H,k} \mathbf{F}_k \mathbf{S}_k\}$. The FIM $\mathbf{J} \in \mathbb{R}^{6U \times 6U}$ of $\boldsymbol{\eta}$:

$$[\mathbf{J}]_{i,j} = \frac{2T\varrho^2}{\sigma^2} \sum_{k=1}^K \text{Re} \left\{ \text{Tr} \left\{ \frac{\partial \bar{\boldsymbol{\mu}}_k^H}{\partial \eta_i} \frac{\partial \bar{\boldsymbol{\mu}}_k}{\partial \eta_j} \right\} \right\},$$

where $i, j = 1, \dots, 6U$ and $\bar{\boldsymbol{\mu}}_k \triangleq \mathbf{W}_H^H \mathbf{H}_{H,k} \mathbf{F}_k$.

- Assuming DL transmissions in M consecutive frames (each frame contains T OFDM symbols from the BS) and focusing on the positioning and tracking performance up to the m -th frame ($m = 1, \dots, M$), the FIM $\tilde{\mathbf{J}}_m \in \mathbb{R}^{4U \times 4U}$ is:

$$\tilde{\mathbf{J}}_m = \mathbf{T}^T \mathbf{J}_m \mathbf{T} + \tilde{\mathbf{J}}_{m-1}.$$

I. Gavras and G. C. Alexandropoulos, "Tracking-aided multi-user MIMO communications with hybrid reconfigurable intelligent surfaces," *arXiv preprint arXiv:2504.18846*, 2025.

PEB Analysis (2/2)

- $\mathbf{T}^T \mathbf{J}_m \mathbf{T}$ and $\tilde{\mathbf{J}}_{m-1}$ represent the FIM with respect to $\tilde{\boldsymbol{\eta}}_m$ and the prior knowledge, respectively.
- The transformation matrix $\mathbf{T} \in \mathbb{R}^{6U \times 4U}$ can be expressed as a Jacobian with $[\mathbf{T}]_{i,j} = \partial[\tilde{\boldsymbol{\eta}}]_i / \partial[\boldsymbol{\eta}]_j$. Note that $\boldsymbol{\eta}_m$ and $\tilde{\boldsymbol{\eta}}_m$ are the channel- and location-domain parameter vectors for the m -th frame and \mathbf{J}_m is computed.
- At the first frame, $\tilde{\mathbf{J}}_0$ is equal to a zero matrix, since no prior knowledge is available yet.
- Combining all the above to quantify the position accuracy up to each m -th frame, we adopt the PEB as our estimation performance metric:

$$\text{PEB}(\mathbf{F}_{\text{TX}}, \mathbf{W}_{\text{H}}; \tilde{\boldsymbol{\eta}}_m) = \sqrt{\text{Tr} \left\{ \tilde{\mathbf{J}}_m^{-1} \right\}}.$$

I. Gavras and G. C. Alexandropoulos, "Tracking-aided multi-user MIMO communications with hybrid reconfigurable intelligent surfaces," *arXiv preprint arXiv:2504.18846*, 2025.

Joint BS and HRIS Design (1/3)

- The BS precoding and HRIS reflection/combining settings are jointly optimized to satisfy QoS constraints for all mobile UEs, while tracking their positions over time to enhance DL transmission. The SINR for the u -th UE, on the k -th subcarrier per OFDM symbol:

$$\text{SINR}_{k,u} = \frac{|\mathbf{h}_{\text{dir},k,u} \mathbf{f}_{k,u}|^2}{\sum_{i=0, i \neq u}^U |\mathbf{h}_{\text{dir},k,u} \mathbf{f}_{k,i}|^2 + \sigma^2},$$

where $\mathbf{h}_{\text{dir},k,u} \triangleq \mathbf{h}_{\text{DL},k,u} + (1 - \rho) \mathbf{h}_{\text{HU},k,u} \text{diag}(\boldsymbol{\varphi}) \mathbf{H}_{\text{BR},k}$, which is composed at each m -th frame $\forall k, u$ using the state estimation for each u -th UE.

- For sensing, at each frame m , directly minimizing the PEB is complex due to high-dimensional constraints; the bound $\text{Tr}\{\tilde{\mathbf{J}}_m^{-1}\} \geq 1/\text{Tr}\{\tilde{\mathbf{J}}_m\}$ can be minimized instead.

I. Gavras and G. C. Alexandropoulos, 'Near-field localization with dynamic metasurface antennas at THz: A CRB minimizing approach,' *IEEE WCL*, 2025.

I. Gavras and G. C. Alexandropoulos, 'Tracking-aided multi-user MIMO communications with hybrid reconfigurable intelligent surfaces,' *arXiv preprint arXiv:2504.18846*, 2025.

Proposed BS and HRIS Design (2/3)

- At each m -th frame, solve:

$$\begin{aligned} \mathcal{OP}_{10}: \max_{\mathbf{F}_{\text{TX}}, \mathbf{W}_H, \varphi} & \text{Tr} \left\{ \tilde{\mathbf{J}}_m \right\} \\ \text{s.t. } & \sum_{k=1}^K \text{SINR}_{k,u} \geq \gamma_u \forall u, \|\mathbf{F}_{\text{TX}}\|^2 \leq P_{\max}, \\ & |w_{l,n}| = 1 \text{ and } |[\phi]_n| = 1 \forall l, n. \end{aligned}$$

- This problem is highly non-convex; an alternating optimization approach has been adopted.

I. Gavras and G. C. Alexandropoulos, "Tracking-aided multi-user MIMO communications with hybrid reconfigurable intelligent surfaces," *arXiv preprint arXiv:2504.18846*, 2025.

Proposed BS and HRIS Design (3/3)

- For a given \mathbf{W}_H and φ , relax as:

$$\begin{aligned} \mathcal{OP}_{11}: & \max_{\{\tilde{\mathbf{F}}_{k,u}\}_{\forall k,u}} \sum_{i=1}^{4U} \sum_{k=1}^K \sum_{u=1}^U \operatorname{Re} \left\{ \operatorname{Tr} \left\{ \mathbf{B}_{k,i} \tilde{\mathbf{F}}_{k,u} \right\} \right\} \\ \text{s.t. } & \sum_{k=1}^K \operatorname{Tr} \left(\mathbf{C}_{k,u} \tilde{\mathbf{F}}_{k,u} \right) - \gamma_u \sum_{i=1, i \neq u}^U \operatorname{Tr} \left(\mathbf{C}_{k,u} \tilde{\mathbf{F}}_{k,i} \right) \geq \gamma_u \sigma^2, \\ & \sum_{k=1}^K \sum_{u=1}^U \|\tilde{\mathbf{F}}_{k,u}\|^2 \leq P_{\max}, \quad \tilde{\mathbf{F}}_{k,u} \succeq 0 \quad \forall k, u, \end{aligned}$$

where $\mathbf{B}_{k,i} \triangleq \frac{\partial \mathbf{H}_{H,k}^H}{\partial \tilde{\eta}_i} \mathbf{W}_H \mathbf{W}_H^H \frac{\partial \mathbf{H}_{H,k}}{\partial \tilde{\eta}_i}$ and $\mathbf{C}_{k,u} \triangleq \mathbf{h}_{\text{dir},k,u}^H \mathbf{h}_{\text{dir},k,u}$.

- This is a convex problem that can be solved efficiently (e.g., CVX).

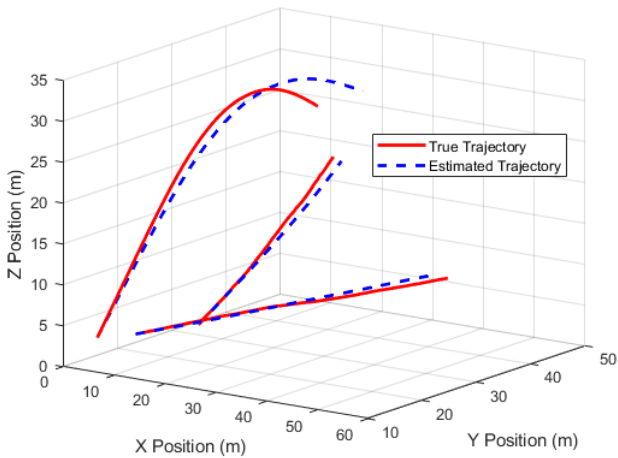
I. Gavras and G. C. Alexandropoulos, "Tracking-aided multi-user MIMO communications with hybrid reconfigurable intelligent surfaces," *arXiv preprint arXiv:2504.18846*, 2025.

Simulation Parameters

- $M = 100$ frames of a wideband setup centered at the 20 GHz frequency, with $K = 32$ subcarriers of $\Delta f = 120$ kHz frequency spacing, where each coherent channel block spanned $T = 200$ OFDM transmissions.
- $U = 3$ mobile UEs, initially placed randomly within $[0, 50]$ meters on the y -axis and $[0, 10]$ meters on the x - and z -axes, with the HRIS at $\mathbf{p}_{\text{RIS}} = [0, 50, 5]$. UE velocities in all directions were randomly set in $[1, 10]$ m/s and kept constant during tracking.
- BS equipped with ULA of $N_T = 16$ antennas and an HRIS with $N_{\text{RF}} = 5$ RX RF chains each connected to $N_E = 8$ hybrid meta-atoms, unless otherwise stated.
- AWGN's variance set as $\sigma^2 = -100$ dBm, the channel coefficients $\beta_k \forall k$ were randomly selected with unit amplitude, $\gamma_u = 10$ dB $\forall u$, and $P_{\max} = 15$ dBm.

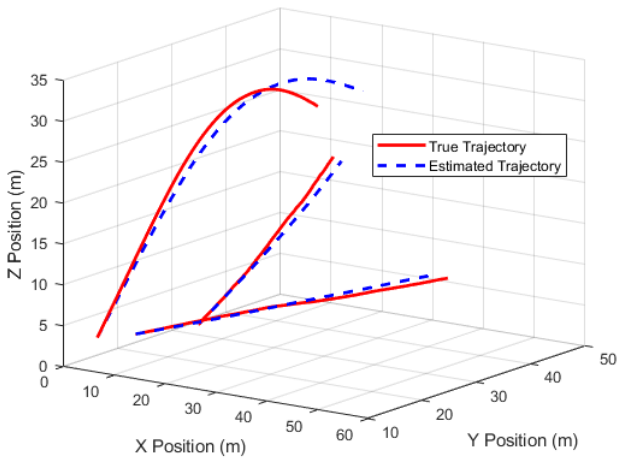
I. Gavras and G. C. Alexandropoulos, "Tracking-aided multi-user MIMO communications with hybrid reconfigurable intelligent surfaces," *arXiv preprint arXiv:2504.18846*, 2025.

True and Estimated Trajectories



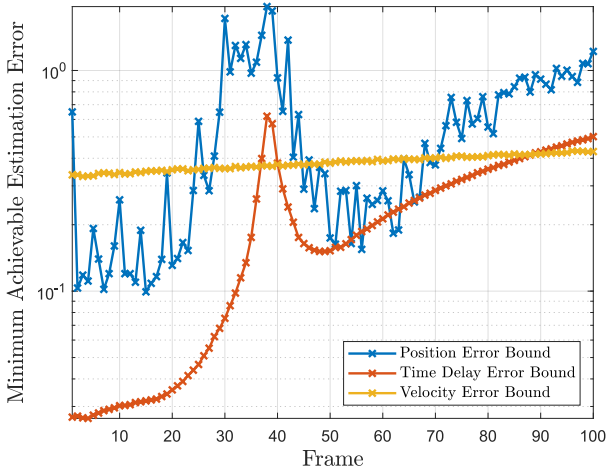
I. Gavras and G. C. Alexandropoulos, "Tracking-aided multi-user MIMO communications with hybrid reconfigurable intelligent surfaces," *arXiv preprint arXiv:2504.18846*, 2025.

True and Estimated Trajectories



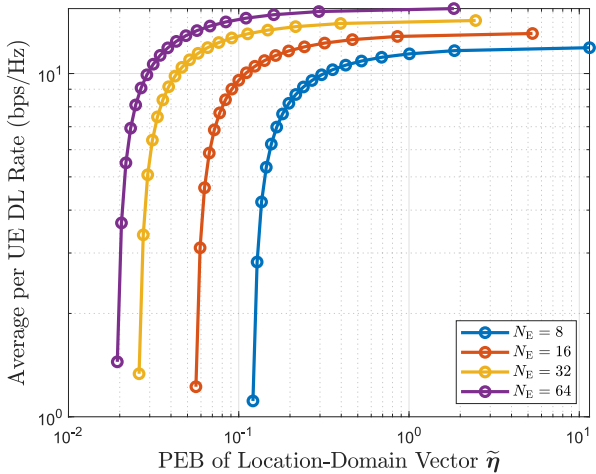
I. Gavras and G. C. Alexandropoulos, "Tracking-aided multi-user MIMO communications with hybrid reconfigurable intelligent surfaces," *arXiv preprint arXiv:2504.18846*, 2025.

Tracking Performance



I. Gavras and G. C. Alexandropoulos, "Tracking-aided multi-user MIMO communications with hybrid reconfigurable intelligent surfaces," *arXiv preprint arXiv:2504.18846*, 2025.

Sensing vs. Communications Performance

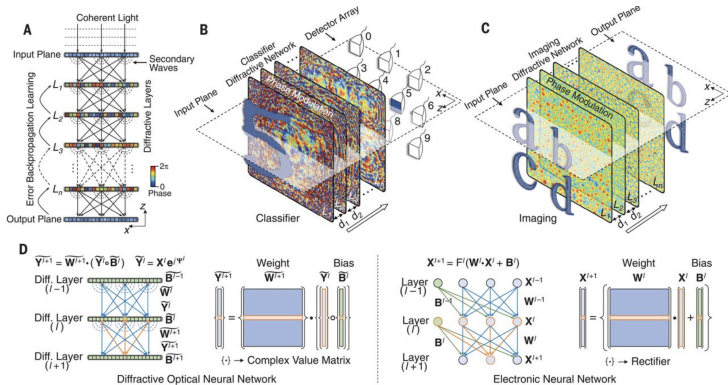


I. Gavras and G. C. Alexandropoulos, "Tracking-aided multi-user MIMO communications with hybrid reconfigurable intelligent surfaces," *arXiv preprint arXiv:2504.18846*, 2025.

1 Part III: Distributed Sensing-Aided Communications

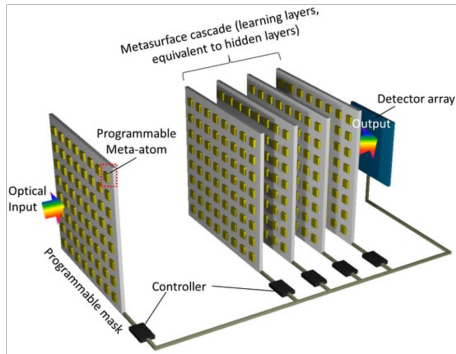
- Optimization of Multi-RIS-Aided Communications
- Distributed Learning for Multi-RIS-Aided Communications
- Position-Aided Near-Field Beam Tracking
- Sensing-Aided Communications via Hydrid RISs
- Over-the-Air Learning: The XL MIMO Potential

Wave-Based Quasi-Optical DNNs



- Metamaterial-based implementations of DNNs have been implemented in controlled testbeds and in the “quasi-optical” RF regime.

SIM as Computational Layers



- Compact layers of diffractive/reflecting RISs; used as XL transceivers for communication; sequential signal flow enables multi-layer nonlinear computing; naturally suited for neural network components.

Z. Jaksic *et al.*, "Synergy between AI and optical metasurfaces: A critical overview of recent advances," *Photonics*, 2024.

J. An, C. Xu, D. W. K. Ng, G. C. Alexandropoulos, C. Huang, C. Yuen, and L. Hanzo, "Stacked intelligent metasurfaces enabling efficient holographic MIMO communications for 6G," *IEEE JSAC*, 2023.

Wave Propagation as Computing

- Wireless propagation can be exploited to perform computations in the wave domain: Over-the-Air Computing (OAC).
- This offers a new paradigm for communications and sensing.
- Different directions for wave-based computing:
 - Wave-based free-space propagation.
 - OAC in multiple access channels.
 - Goal-Oriented Communications (GOC).

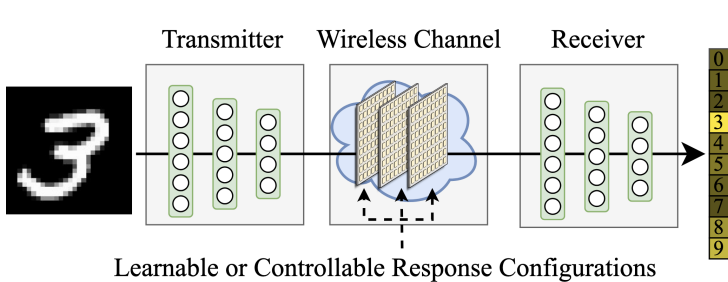
- Metamaterial-based implementations of DNNs have been implemented in controlled testbeds and in the “quasi-optical” RF regime.
- Federated learning approaches have been used to aggregate DNN weights in OAC style for multi-user wireless communication systems.
- GOC is implemented by splitting the layers of a DNN at the TX and the RX and transmit intermediate layer outputs, while possibly accounting for reconfiguration of the wireless environment using RISs.

- ① OAC and wave-based computing rarely account for practical (even static) fading conditions.
- ② GOC require extensive training to account for dynamic fading (even with RISs that control the environment) and are less successful in rich scattering environments.
- ③ None of the approaches are fully analog, since they require digital processing at the transceivers.

- A communication/computation problem where the RX only wants to estimate (infer) a property of the TX's data (e.g., sensing result).
- Three ways to treat it:
 - ① “Transmit-then-infer”: TX sends data, RX computes; high communication resources, low computation at the Xx side.
 - ② “Infer-then-transmit”: TX performs computations and transmits the result.
 - ③ “Infer-while-transmitting”: The layers of a DNN are split across the endpoints. Intermediate representations are transmitted, while simultaneously accounting for channel effects.

- The wireless channel is typically treated as a source of noise.
- Most approaches aim at negating its effects by reconstructing the transmitted signal at the Rx before proceeding with its computation.
 - Computationally wasteful.
 - Signal reconstruction is not the objective.
- When the channel is controllable (i.e., via RISs), propagation effects can be used to perform computation instead.

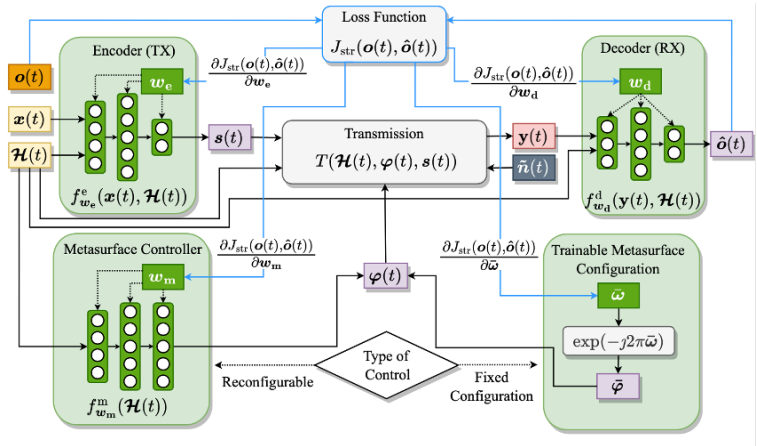
Metasurfaces-Integrated NNs (MINNs)



- Sequential diffractions from SIM (or RISs) devices mimic the operations of hidden DNN layers; potential for ISAC.

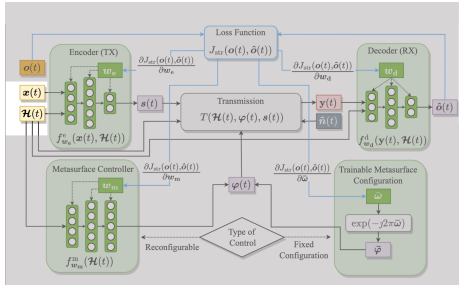
K. Stylianopoulos, P. Di Lorenzo, and G. C. Alexandropoulos, "Over-the-air edge inference via end-to-end metasurfaces-integrated artificial neural networks," *arXiv preprint:2504.00233*, 2025.

The MINN Architecture



K. Stylianopoulos, P. Di Lorenzo, and G. C. Alexandropoulos, "Over-the-air edge inference via end-to-end metasurfaces-integrated artificial neural networks," *arXiv preprint:2504.00233*, 2025.

MINN Training (1/6)



Algorithm 1 Training of the proposed E2E MINN with trainable MS responses

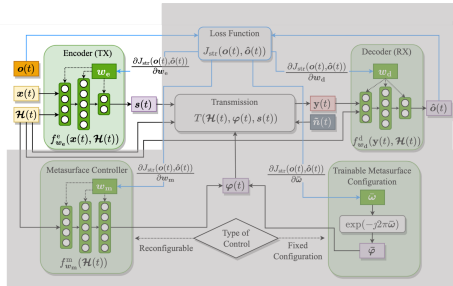
```

1: Construct combined DNN weight vector  $\mathbf{w}$  of the TX/RX/MS modules as:
2:    $\mathbf{w} = \text{concat}(\mathbf{w}_d, \mathbf{w}_e, \bar{\mathbf{w}})$ .                                ▷ Trainable MS configuration  $\bar{\mathbf{w}}$ 
3: Initialize  $\mathbf{w}$  randomly.
4: for  $t = 1, 2, \dots$ , until convergence do
5:   Sample input-target data  $(\mathbf{x}(t), \mathbf{o}(t))$  from data set.
6:   Sample channel realization  $\mathcal{H}(t)$  from collected measurements.
7:   Compute transmitted signal  $s(t)$  as:
8:      $s(t) = f_{w_e}^e(\mathbf{x}(t), \mathcal{H}(t))$ .                                ▷  $\mathcal{H}$  is ignored for channel-agnostic encoder
9:   Compute MS response  $\phi(t) = \exp(-j2\pi\bar{\omega})$  for RIS (and similar for SIM).
10:  Transmit  $s(t)$  to receive signal  $y(t)$  as:
11:     $y(t) = T(\mathcal{H}(t), \phi(t), s(t))$ .                                ▷ Channel is a function of the controllable  $\phi(t)$ 
12:  Get output estimate  $\hat{o}(t)$  as:
13:     $\hat{o}(t) = f_{w_d}^d(y(t), \mathcal{H}(t))$ .                                ▷  $\mathcal{H}$  is ignored for channel-agnostic decoder
14:  Calculate error  $l(t)$  based on loss function  $J$  as:
15:     $l(t) = J(\mathbf{o}(t), \hat{\mathbf{o}}(t))$                                          ▷  $\mathbf{o}(t)$  is the ground truth label
16:  Set  $\mathbf{w} \leftarrow \mathbf{w} - \eta \nabla_{\mathbf{w}} l(t)$                                          ▷ Gradient updates through backpropagation
17: end for
18: Return  $\mathbf{w}$ 

```

K. Stylianopoulos, P. Di Lorenzo, and G. C. Alexandropoulos, "Over-the-air edge inference via end-to-end metasurfaces-integrated artificial neural networks," *arXiv preprint:2504.00233*, 2025.

MINN Training (2/6)



Algorithm 1 Training of the proposed E2E MINN with trainable MS responses

```

1: Construct combined DNN weight vector  $\mathbf{w}$  of the TX/RX/MS modules as:  

2:  $\mathbf{w} = \text{concat}(\mathbf{w}_e, \mathbf{w}_o, \tilde{\mathbf{w}})$ . ▷ Trainable MS configuration  $\tilde{\mathbf{w}}$   

3: Initialize  $\mathbf{w}$  randomly.  

4: for  $t = 1, 2, \dots$ , until convergence do  

5: Sample input-target data  $(\mathbf{x}(t), \mathbf{o}(t))$  from data set.  

6: Sample channel realization  $\mathcal{H}(t)$  from collected measurements.  

7: Compute transmitted signal  $\mathbf{s}(t)$  as:  

8:  $\mathbf{s}(t) = f_{w_e}^e(\mathbf{x}(t), \mathcal{H}(t))$ . ▷  $\mathcal{H}$  is ignored for channel-agnostic encoder  

9: Compute MS response  $\varphi(t) = \exp(-j2\pi\omega)$  for RIS (and similar for SIM).  

10: Transmit  $\mathbf{s}(t)$  to receive signal  $\mathbf{y}(t)$  as:  

11:  $\mathbf{y}(t) = T(\mathcal{H}(t), \varphi(t), \mathbf{s}(t))$ . ▷ Channel is a function of the controllable  $\varphi(t)$   

12: Get output estimate  $\hat{\mathbf{o}}(t)$  as:  

13:  $\hat{\mathbf{o}}(t) = f_{w_d}^d(\mathbf{y}(t), \mathcal{H}(t))$ . ▷  $\mathcal{H}$  is ignored for channel-agnostic decoder  

14: Calculate error  $l(t)$  based on loss function  $J$  as:  

15:  $l(t) = J(\mathbf{o}(t), \hat{\mathbf{o}}(t))$  ▷  $\mathbf{o}(t)$  is the ground truth label  

16: Set  $\mathbf{w} \leftarrow \mathbf{w} - \eta \nabla l(t)$  ▷ Gradient updates through backpropagation  

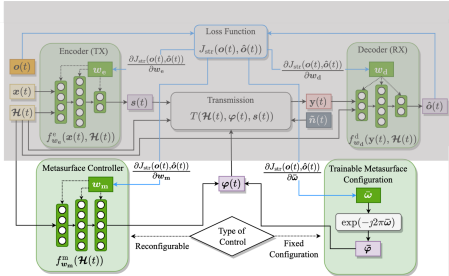
17: end for  

18: Return  $\mathbf{w}$ 

```

K. Stylianopoulos, P. Di Lorenzo, and G. C. Alexandropoulos, "Over-the-air edge inference via end-to-end metasurfaces-integrated artificial neural networks," *arXiv preprint:2504.00233*, 2025.

MINN Training (3/6)



Algorithm 1 Training of the proposed E2E MINN with trainable MS responses

```

1: Construct combined DNN weight vector  $\mathbf{w}$  of the TX/RX/MS modules as:  

2:  $\mathbf{w} = \text{concat}(\mathbf{w}_e, \mathbf{w}_o, \bar{\omega})$ . ▷ Trainable MS configuration  $\bar{\omega}$   

3: Initialize  $\mathbf{w}$  randomly.  

4: for  $t = 1, 2, \dots$ , until convergence do  

5:   Sample input-target data  $(\mathbf{x}(t), \mathbf{o}(t))$  from data set.  

6:   Sample channel realization  $\mathcal{H}(t)$  from collected measurements.  

7:   Compute transmitted signal  $s(t)$  as:  

8:      $s(t) = f_{w_e}^e(\mathbf{x}(t), \mathcal{H}(t))$ . ▷  $\mathcal{H}$  is ignored for channel-agnostic encoder  

9:   Compute MS response  $\varphi(t) = \exp(-j2\pi\bar{\omega})$  for RIS (and similar for SIM).  

10:  Transmit  $s(t)$  to receive signal  $\mathbf{y}(t)$  as:  

11:     $\mathbf{y}(t) = \mathcal{T}(\mathcal{H}(t), \varphi(t), s(t))$ . ▷ Channel is a function of the controllable  $\varphi(t)$   

12:  Get output estimate  $\hat{\mathbf{o}}(t)$  as:  

13:     $\hat{\mathbf{o}}(t) = f_{w_o}^d(\mathbf{y}(t), \mathcal{H}(t))$ . ▷  $\mathcal{H}$  is ignored for channel-agnostic decoder  

14:  Calculate error  $l(t)$  based on loss function  $J$  as:  

15:     $l(t) = J(\mathbf{o}(t), \hat{\mathbf{o}}(t))$ . ▷  $\mathbf{o}(t)$  is the ground truth label  

16:  Set  $\mathbf{w} \leftarrow \mathbf{w} - \eta \nabla l(t)$  ▷ Gradient updates through backpropagation  

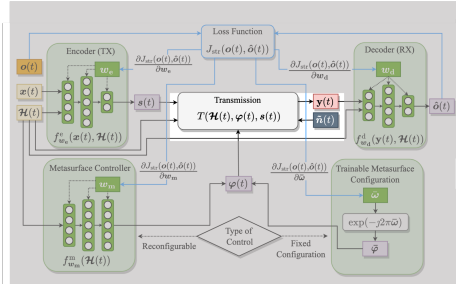
17: end for  

18: Return  $\mathbf{w}$ 

```

K. Stylianopoulos, P. Di Lorenzo, and G. C. Alexandropoulos, "Over-the-air edge inference via end-to-end metasurfaces-integrated artificial neural networks," *arXiv preprint:2504.00233*, 2025.

MINN Training (4/6)



Algorithm 1 Training of the proposed E2E MINN with trainable MS responses

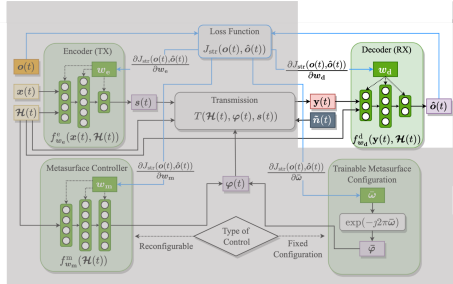
```

1: Construct combined DNN weight vector  $\mathbf{w}$  of the TX/RX/MS modules as:
2:    $\mathbf{w} = \text{concat}(\mathbf{w}_e, \mathbf{w}_d, \bar{\omega})$ .                                ▷ Trainable MS configuration  $\bar{\omega}$ 
3: Initialize  $\mathbf{w}$  randomly.
4: for  $t = 1, 2, \dots$ , until convergence do
5:   Sample input-target data  $(\mathbf{x}(t), \mathbf{o}(t))$  from data set.
6:   Sample channel realization  $\mathcal{H}(t)$  from collected measurements.
7:   Compute transmitted signal  $s(t)$  as:
8:      $s(t) = f_{w_e}^o(\mathbf{x}(t), \mathcal{H}(t))$ .                                ▷  $\mathcal{H}$  is ignored for channel-agnostic encoder
9:   Compute MS response  $\phi(t) = \exp(-j2\pi\bar{\omega})$  for RIS (and similar for SiM).
10:  Transmit  $s(t)$  to receive signal  $\mathbf{y}(t)$  as:
11:     $\mathbf{y}(t) = \mathcal{T}(\mathcal{H}(t), \phi(t), s(t))$ .                                ▷ Channel is a function of the controllable  $\phi(t)$ 
12:  Get output estimate  $\hat{\mathbf{o}}(t)$  as:
13:     $\hat{\mathbf{o}}(t) = f_{w_d}^o(\mathbf{y}(t), \mathcal{H}(t))$ .                                ▷  $\mathcal{H}$  is ignored for channel-agnostic decoder
14:  Calculate error  $l(t)$  based on loss function  $J$  as:
15:     $l(t) = J(\mathbf{o}(t), \hat{\mathbf{o}}(t))$ .                                         ▷  $\mathbf{o}(t)$  is the ground truth label
16:  Set  $\mathbf{w} \leftarrow \mathbf{w} - \eta \nabla_{\mathbf{w}} l(t)$                                          ▷ Gradient updates through backpropagation
17: end for
18: Return  $\mathbf{w}$ 

```

K. Stylianopoulos, P. Di Lorenzo, and G. C. Alexandropoulos, "Over-the-air edge inference via end-to-end metasurfaces-integrated artificial neural networks," *arXiv preprint:2504.00233*, 2025.

MINN Training (5/6)



Algorithm 1 Training of the proposed E2E MINN with trainable MS responses

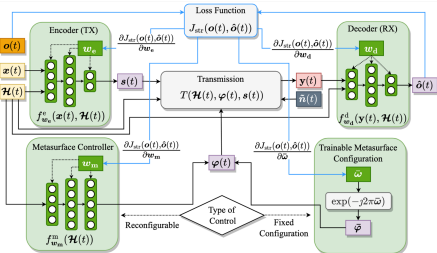
```

1: Construct combined DNN weight vector  $\mathbf{w}$  of the TX/RX/MS modules as:
2:    $\mathbf{w} = \text{concat}(\mathbf{w}_d, \mathbf{w}_e, \bar{\omega})$ .                                ▷ Trainable MS configuration  $\bar{\omega}$ 
3: Initialize  $\mathbf{w}$  randomly.
4: for  $t = 1, 2, \dots$ , until convergence do
5:   Sample input-target data  $(\mathbf{x}(t), \mathbf{o}(t))$  from data set.
6:   Sample channel realization  $\mathcal{H}(t)$  from collected measurements.
7:   Compute transmitted signal  $\mathbf{s}(t)$  as:
8:      $\mathbf{s}(t) = f_{w_e}^e(\mathbf{x}(t), \mathcal{H}(t))$ .                                ▷  $\mathcal{H}$  is ignored for channel-agnostic encoder
9:   Compute MS response  $\phi(t) = \exp(-j2\pi\bar{\omega})$  for RIS (and similar for SIM).
10:  Transmit  $\mathbf{s}(t)$  to receive signal  $\mathbf{y}(t)$  as:
11:     $\mathbf{y}(t) = T(\mathcal{H}(t), \phi(t), \mathbf{s}(t))$ .                                ▷ Channel is a function of the controllable  $\phi(t)$ 
12:  Get output estimate  $\hat{\mathbf{o}}(t)$  as:
13:     $\hat{\mathbf{o}}(t) = f_{w_d}^d(\mathbf{y}(t), \mathcal{H}(t))$ .                                ▷  $\mathcal{H}$  is ignored for channel-agnostic decoder
14:  Calculate error  $l(t)$  based on loss function  $J$  as:
15:     $l(t) = J(\mathbf{o}(t), \hat{\mathbf{o}}(t))$                                               ▷  $\mathbf{o}(t)$  is the ground truth label
16:  Set  $\mathbf{w} \leftarrow \mathbf{w} - \eta \nabla_{\mathbf{w}} l(t)$                                          ▷ Gradient updates through backpropagation
17: end for
18: Return  $\mathbf{w}$ 

```

K. Stylianopoulos, P. Di Lorenzo, and G. C. Alexandropoulos, "Over-the-air edge inference via end-to-end metasurfaces-integrated artificial neural networks," *arXiv preprint:2504.00233*, 2025.

MINN Training (6/6)



Algorithm 1 Training of the proposed E2E MINN with trainable MS responses

```

1: Construct combined DNN weight vector  $\mathbf{w}$  of the TX/RX/MS modules as:
2:    $\mathbf{w} = \text{concat}(\mathbf{w}_e, \mathbf{w}_o, \bar{\omega})$ .                                ▷ Trainable MS configuration  $\bar{\omega}$ 
3: Initialize  $\mathbf{w}$  randomly.
4: for  $t = 1, 2, \dots$ , until convergence do
5:   Sample input-target data  $(\mathbf{x}(t), \mathbf{o}(t))$  from data set.
6:   Sample channel realization  $\mathcal{H}(t)$  from collected measurements.
7:   Compute transmitted signal  $s(t)$  as:
8:      $s(t) = f_{w_e}^e(\mathbf{x}(t), \mathcal{H}(t))$ .                                ▷  $\mathcal{H}$  is ignored for channel-agnostic encoder
9:   Compute MS response  $\phi(t) = \exp(-j2\pi\bar{\omega})$  for RIS (and similar for SIM).
10:  Transmit  $s(t)$  to receive signal  $\mathbf{y}(t)$  as:
11:     $\mathbf{y}(t) = T(\mathcal{H}(t), \phi(t), s(t))$ .                                ▷ Channel is a function of the controllable  $\phi(t)$ 
12:  Get output estimate  $\hat{\delta}(t)$  as:
13:     $\hat{\delta}(t) = f_{w_d}^d(\mathbf{y}(t), \mathcal{H}(t))$ .                                ▷  $\mathcal{H}$  is ignored for channel-agnostic decoder
14:  Calculate error  $l(t)$  based on loss function  $J$  as:
15:     $l(t) = J(\mathbf{o}(t), \hat{\delta}(t))$                                          ▷  $\mathbf{o}(t)$  is the ground truth label
16:  Set  $\mathbf{w} \leftarrow \mathbf{w} - \eta \nabla_{\mathbf{w}} l(t)$                                          ▷ Gradient updates through backpropagation
17: end for
18: Return  $\mathbf{w}$ 

```

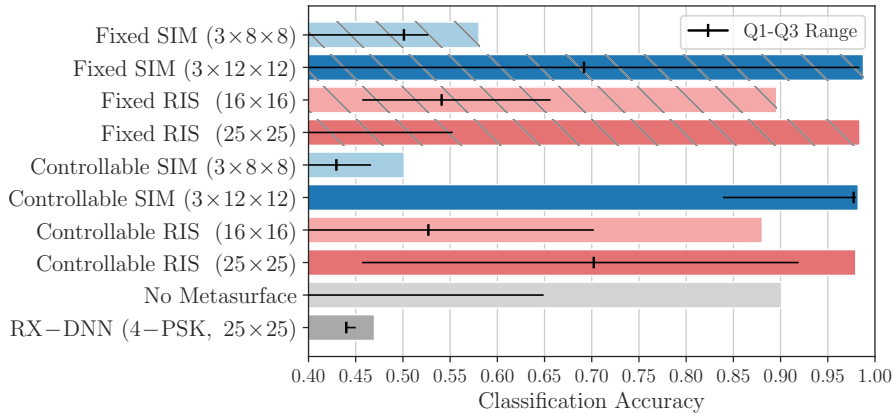
K. Stylianopoulos, P. Di Lorenzo, and G. C. Alexandropoulos, "Over-the-air edge inference via end-to-end metasurfaces-integrated artificial neural networks," *arXiv preprint:2504.00233*, 2025.

Simulation Parameters

- MIMO system with dynamic Ricean fading.
- MNIST images are used as TX input data $\mathbf{x}(t)$. The RX aims to retrieve the numeric digit values $\mathbf{o}(t)$.
- LOS-dominant conditions with i.i.d. channel realizations.
- Shallow CNN and MLP modules as encoders, decoders, and controllers of the metasurfaces.
- Comparisons between:
 - Channel aware vs. channel agnostic modules.
 - RISs vs. SIM.
 - Metasurfaces with a static (but trainable) response vs. reconfigurable responses.

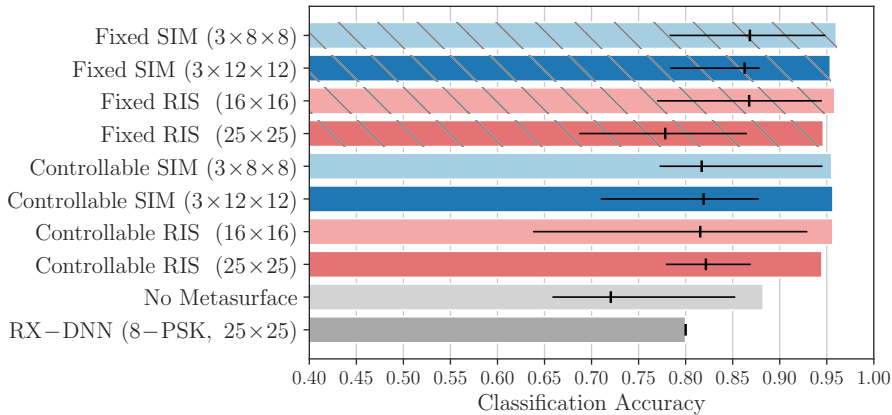
K. Stylianopoulos, P. Di Lorenzo, and G. C. Alexandropoulos, "Over-the-air edge inference via end-to-end metasurfaces-integrated artificial neural networks," *arXiv preprint:2504.00233*, 2025.

Controllable vs. Fixed SIM/RISs with CSI, $N_t = 4$



K. Stylianopoulos, P. Di Lorenzo, and G. C. Alexandropoulos, "Over-the-air edge inference via end-to-end metasurfaces-integrated artificial neural networks," *arXiv preprint:2504.00233*, 2025.

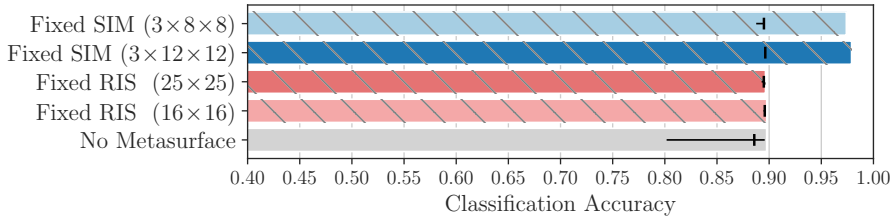
Controllable vs. Fixed SIM/RISs with CSI, $N_t = 12$



No discernible difference between controllable and fixed metasurfaces; SIM and RISs with the same elements have equal performance; the size of the RIS/SIM is the most important factor; in larger antenna numbers, all variations are successful.

K. Stylianopoulos, P. Di Lorenzo, and G. C. Alexandropoulos, "Over-the-air edge inference via end-to-end metasurfaces-integrated artificial neural networks," *arXiv preprint:2504.00233*, 2025.

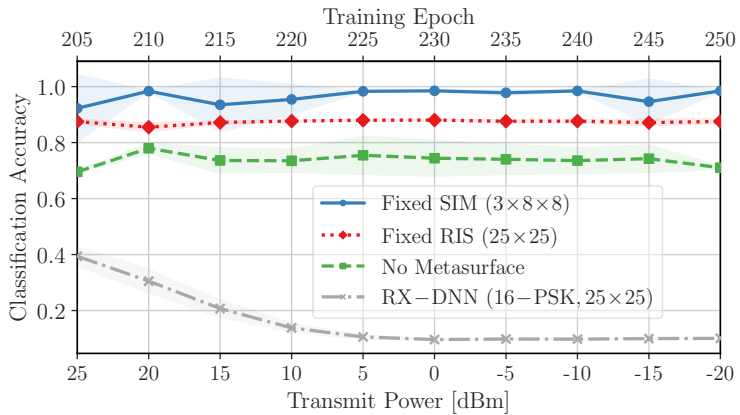
CSI-Agnostic Variations with Fixed SIM/RISs, $N_t = 6$



In the absence of channel information, SIM devices are more efficient than their RIS counterparts.

K. Stylianopoulos, P. Di Lorenzo, and G. C. Alexandropoulos, "Over-the-air edge inference via end-to-end metasurfaces-integrated artificial neural networks," *arXiv preprint:2504.00233*, 2025.

Fine-Tuning Training vs. Decreasing TX Power



MINN is initially trained with high SNR data, power is reduced gradually during training; its performance is robust across a wide range of SNR levels.

K. Stylianopoulos, P. Di Lorenzo, and G. C. Alexandropoulos, "Over-the-air edge inference via end-to-end metasurfaces-integrated artificial neural networks," *arXiv preprint:2504.00233*, 2025.

- GOC approaches, even with the integration of metasurfaces, exhibit slow training.
- Rich scattering fading is often detrimental in training.
- How well do metasurface-based layers perform? Any theoretical guarantees in terms of function approximation?
- Need for digital processing layers at TX/RX despite the metasurface-based layers.

XL MIMO as Extreme Learning Machines

- MIMO systems can be treated as two-layer DNNs, under the conditions:
 - ① Large antenna regimes (XL MIMO);
 - ② Analog combining at the RX with non-linear elements; and
 - ③ Sufficiently rich scattering on the propagation environment.
- When these conditions hold, an XL MIMO system can be casted to the framework of ELMs, thus, it can serve as an analog universal approximator computer.
- **Benefits:** Closed-form training, easy to adapt in dynamic fading; and no processing at the TX, only analog combining at the RX.

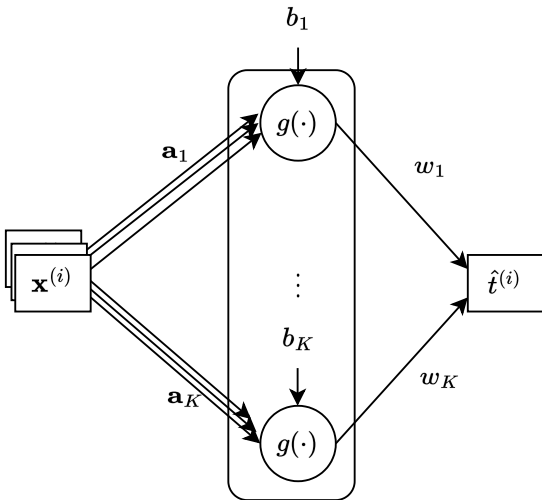
K. Stylianopoulos and G. C. Alexandropoulos, "Universal approximation with XL MIMO systems: OTA classification via trainable analog combining," *arXiv preprint:2504.12758*, 2025.

Theory of Extreme Learning Machines (1/3)

- Data set of input-target pairs $\mathcal{D} \triangleq \{(\mathbf{x}^{(i)}, t^{(i)})\}_{i=1}^D$, where $\forall i$:
 $\mathbf{x}^{(i)} \triangleq [x_1^{(i)}, x_2^{(i)}, \dots, x_d^{(i)}]^\top \in \mathbb{R}^{d \times 1}$.
- ELM ingredients:
 - K hidden nodes in the first layer with random coefficients:
 $\mathbf{A} \triangleq [\mathbf{a}_1, \dots, \mathbf{a}_K]^\top \in \mathbb{R}^{K \times d}$ with $\mathbf{a}_k \in \mathbb{R}^{d \times 1}$; and
 $\mathbf{b} \triangleq [b_1, \dots, b_K]^\top \in \mathbb{R}^{K \times 1}$.
 - An activation function $g(\cdot)$ which is *i*) arbitrary non-linear; *ii*) bounded; *iii*) infinitely differentiable; and *iv*) convergent.
 - K trainable weights $\mathbf{w} \triangleq [w_1, w_2, \dots, w_K]^\top \in \mathbb{R}^{K \times 1}$ on the output layer that perform weighted averaging on the outputs of the activations, i.e., $\forall i$:

$$\hat{t}^{(i)} \triangleq \sum_{k=1}^K w_k g\left(\mathbf{a}_k^\top \mathbf{x}^{(i)} + b_k\right) = \mathbf{w}^\top g\left(\bar{\mathbf{A}} \bar{\mathbf{x}}^{(i)}\right).$$

Theory of Extreme Learning Machines (2/3)



Theory of Extreme Learning Machines (3/3)

- Training an ELM involves finding appropriate values for w_k 's; this is formulated as an MSE objective over the data set:

$$\mathbf{w}^* \triangleq \operatorname{argmin}_{\mathbf{w}} \|\mathbf{G}\mathbf{w} - \mathbf{t}\|,$$

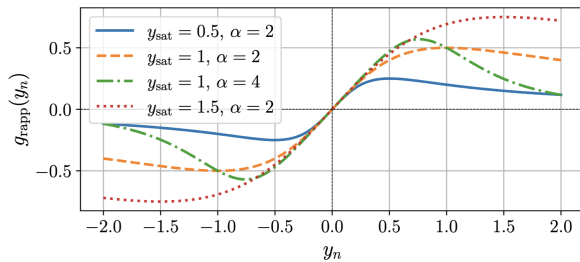
where \mathbf{G} is the output of the activations of ELM's first layer for the whole data set and \mathbf{t} is their corresponding target values.

- LS solution: $\mathbf{w}^* = \mathbf{G}^\dagger \mathbf{t}$.
- **Universal Approximation Theorem:** If the random coefficients are i.i.d. and with infinite support, then, for any valid $g(\cdot)$, there exists a hidden layer size $K < D$ that the LS solution gives an arbitrarily small error.

MIMO and Nonlinear Analog Combining

- Received signal model: $\mathbf{y} \triangleq \mathbf{H}\mathbf{s} + \tilde{\mathbf{n}}$
- Soft-thresholding operation at each n -th RX RF chain via Rapp's model for nonlinear active elements (e.g., power amplifiers):

$$g_{\text{rapp}}(y_n) \triangleq y_n (1 + (y_n/y_{\text{sat}})^{\alpha})^{-1}.$$



K. Stylianopoulos and G. C. Alexandropoulos, "Universal approximation with XL MIMO systems: OTA classification via trainable analog combining," *arXiv preprint:2504.12758*, 2025.

- End-to-end MIMO reception:

$\textcolor{red}{z} \triangleq \sum_{n=1}^{N_r} q_n g_{\text{rapp}}(y_n) = \mathbf{q}^\top \textcolor{orange}{g}_{\text{rapp}}(\textcolor{green}{\text{Re}\{\mathbf{H}\}} \bar{\mathbf{x}})$, with $\mathbf{q} \triangleq [q_1, \dots, q_{N_r}]^\top$ being the analog combiner.

- It's easy to see that: $\hat{\mathbf{t}}^{(i)} \triangleq \sum_{k=1}^K w_k g \left(\mathbf{a}_k^\top \mathbf{x}^{(i)} + b_k \right) = \mathbf{w}^\top \textcolor{orange}{g} \left(\bar{\mathbf{A}} \bar{\mathbf{x}}^{(i)} \right)$, hence an XL MIMO system can be seen as an ELM:

- The combined signal z plays the role of the ELM's output $\hat{\mathbf{t}}^{(i)}$.
- Each component of the input vector $\bar{\mathbf{x}}^{(i)}$ is transmitted by a different TX antenna.
- \mathbf{H} plays the role of the random hidden layer coefficients (for rich scattering).
- The Rapp activation function plays the role of the activation.
- The analog combining weights \mathbf{q} are the only trainable components.

K. Stylianopoulos and G. C. Alexandropoulos, "Universal approximation with XL MIMO systems: OTA classification via trainable analog combining," *arXiv preprint:2504.12758*, 2025.

Evaluation on Classification Data Sets

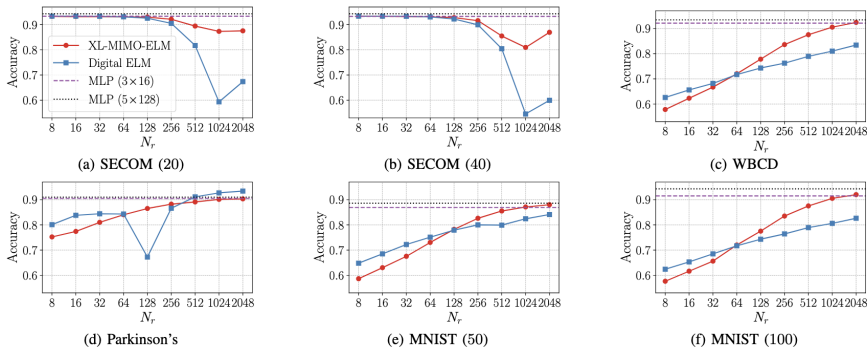
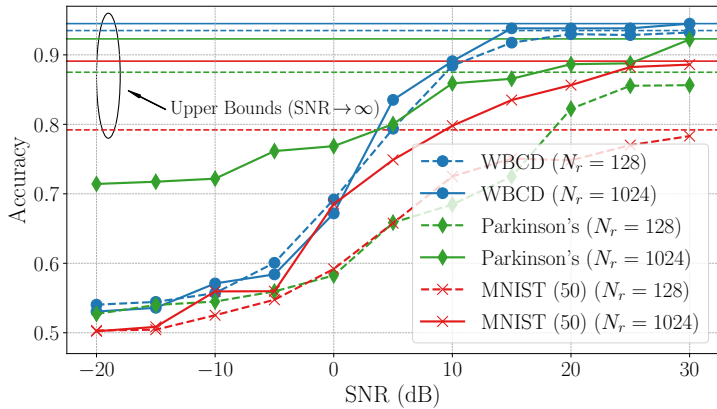


Fig. 2: Comparative performance of the proposed XL-MIMO-ELM with benchmarks across different datasets for increasing number of Rx antennas N_r (implying the number of units in the hidden layer).

XL-MIMO-ELM achieves equal performance to its fully digital counterparts; both ELM versions reach the performance of DNN benchmarks (that require iterative training).

K. Stylianopoulos and G. C. Alexandropoulos, "Universal approximation with XL MIMO systems: OTA classification via trainable analog combining," *arXiv preprint:2504.12758*, 2025.

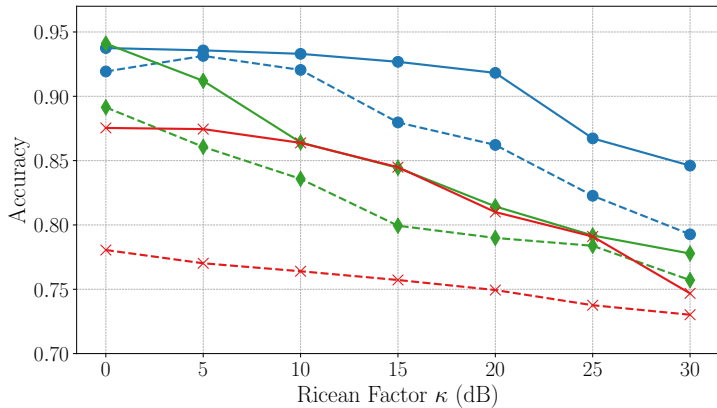
Impact of Noise



In the high-SNR regime, XL-MIMO-ELMs achieve their optimal performance, validating the exclusion of noise in the theoretical treatment.

K. Stylianopoulos and G. C. Alexandropoulos, "Universal approximation with XL MIMO systems: OTA classification via trainable analog combining," *arXiv preprint:2504.12758*, 2025.

Impact of Channel Diversity



XL-MIMO-ELMs are more effective in rich scattering conditions, as the channel provides high diversity to satisfy the requirements of the universal approximation theorem.

K. Stylianopoulos and G. C. Alexandropoulos, "Universal approximation with XL MIMO systems: OTA classification via trainable analog combining," *arXiv preprint:2504.12758*, 2025.

Ongoing Work

- Metasurface design for wave-domain non-linearities and combining.
- Multi-layer architectures.
- Controllable channel responses using metasurfaces.
- Combiner optimization to achieve data detection simultaneous to inference: optimize the combiner to maximize a dual objective of MSE (for ELM learning) and capacity (for data transmission).

K. Stylianopoulos and G. C. Alexandropoulos, "Universal approximation with XL MIMO systems: OTA classification via trainable analog combining," *arXiv preprint:2504.12758*, 2025.

Acknowledgements

- JU-SNS-2022 project TERRAMETA, terrameta-project.eu.
- JU-SNS-2023 project 6G-DISAC, 6gdisac-project.eu.



Thank you for your attention

Prof. George C. Alexandropoulos

e-mail: alexandg@di.uoa.gr

URL: www.alexandropoulos.info

